International Journal of Optics

Modelling of Non-Linear Optical Signal Processing Devices and Systems

Lead Guest Editor: Bhagwan Das
Guest Editors: Mohammad Faiz Liew Abdullah and Yuanchun Zhou

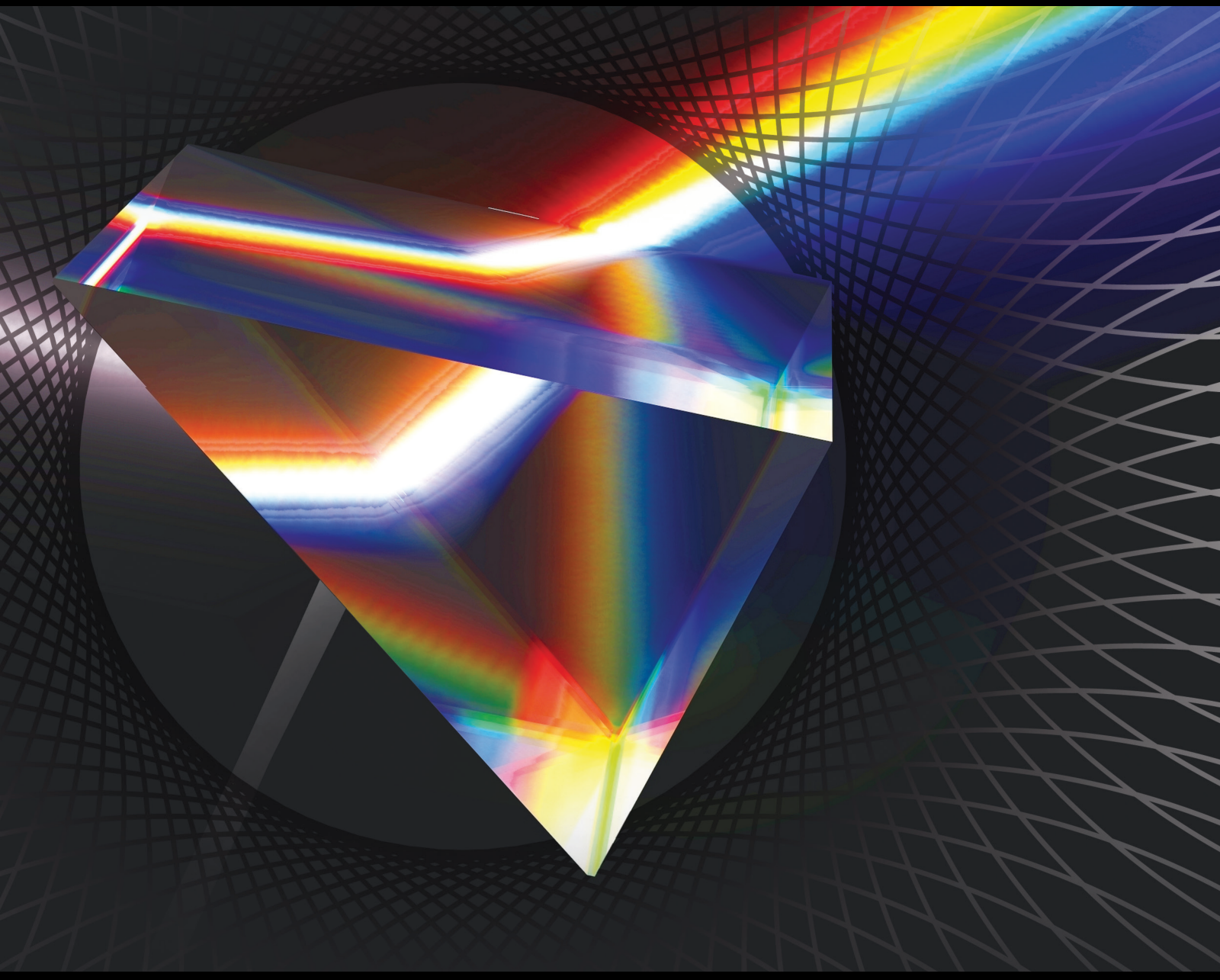

Modelling of Non-Linear Optical Signal Processing Devices and Systems

International Journal of Optics

Modelling of Non-Linear Optical Signal Processing Devices and Systems

Lead Guest Editor: Bhagwan Das
Guest Editors: Mohammad Faiz Liew Abdullah and Yuanchun Zhou

Contents

Hindawi
International Journal of Optics
Volume 2022, Article ID 6085833, 9 pages
https://doi.org/10.1155/2022/6085833

Research Article

Design and Bulk Sensitivity Analysis of a Silicon Nitride Photonic Biosensor for Cancer Cell Detection

Prasanna Kumaar S. and Sivabramanian A.

School of Electronics Engineering, Vellore Institute of Technology, Chennai 600127, India

Correspondence should be addressed to Sivabramanian A.; sivasubramanian.a@vit.ac.in

Received 19 January 2022; Revised 24 March 2022; Accepted 11 April 2022; Published 25 May 2022

Academic Editor: Bhagwan Das

Bulk sensitivity is an important parameter to validate the efficiency of the photonic waveguide sensor. Due to recent advancements in point-of-care silicon photonic biosensing, the focus is to identify the effective way to improve sensitivity. Integrating polydimethylsiloxane (PDMS) microfluidic channel in sensor architecture decreases the sensitivity due to leakage of molecules at edges. The silicon nitride (SiN4) Mach–Zehnder interferometer utilizes the refractive index of different cancer cells (1.39–1.401) to determine the bulk sensitivity. The proposed gradient step rib-slot structure of 970 nm wide and 400 nm thickness is designed to hold the liquid sample without any PDMS material. This novel waveguide exhibits high waveguide bulk sensitivity $S_{w,\text{bulk}}$ and device bulk sensitivity S_d compared with the gradient rib waveguide. We achieved a waveguide bulk sensitivity ($S_{w,\text{bulk}}$) of 2.0699 RIU/RIU and device sensitivity (S_d) of 568 nm/RIU through finite-difference time-domain (FDTD) analysis.

1. Introduction

Virus has been a significant outbreak in recent times. Interest in label-free biosensors has increased due to the diagnosis techniques used in postpandemic [1]. Cancer is the most severe disease globally at present [2]. There are more than 100 different types of cancer group cells that will affect every organ in a body [3]. Early detection of cancer in postpandemic is most important in current diagnosis and medication techniques [4]. Due to its rapid detection and high sensitivity capability, low-cost label-free point-of-care biosensors are developed [5]. Many research findings were reported in the literature on detection of target molecules in biological and environmental applications [6, 7]. Biosensors can be classified based on transduction mechanisms such as electrochemical, electro-optical, optical, mechanical, acoustical, chemical-immunoassays, spectroscopy [8], and image processing algorithms [9, 10]. In an optical method, no-chemical reagents are added to the sample [11]. This will increase the sensitivity to quantify the biomolecule present in the sample [12]. In future, the point-of-care devices may be integrated with mobile phones [13]. By considering all these parameters, we chose a silicon photonic waveguide biosensor [14].

This silicon-based photonic device can be easily fabricated using the available CMOS foundry. This platform offers a wide variety of optimization based on application. The optimization may be waveguide geometry, spectrum analyzer, CCD (charge coupled device) detector, light sources, etc. [15]. For cancer cell detection, the main challenges are absorption of a biomolecule into the waveguide [16]. Integrating polydimethylsiloxane (PDMS) microfluidic channel in sensor architecture decreases the sensitivity due to leakage of molecules at edges. Silicon nitride waveguides are preferred as they offer low waveguide loss and are flexible in fabrication compared with silicon-on-insulator (SOI) waveguides [17, 18]. Some recent reports on fabrication up to 900 nm thickness are done without any cracking stress on silicon nitride [19]. Mach–Zehnder interferometer (MZI) exhibits good response for the cancer blood cell as MZI sensing arm has long length interaction over the sample, and dynamic waveguide structures are integrated [20].

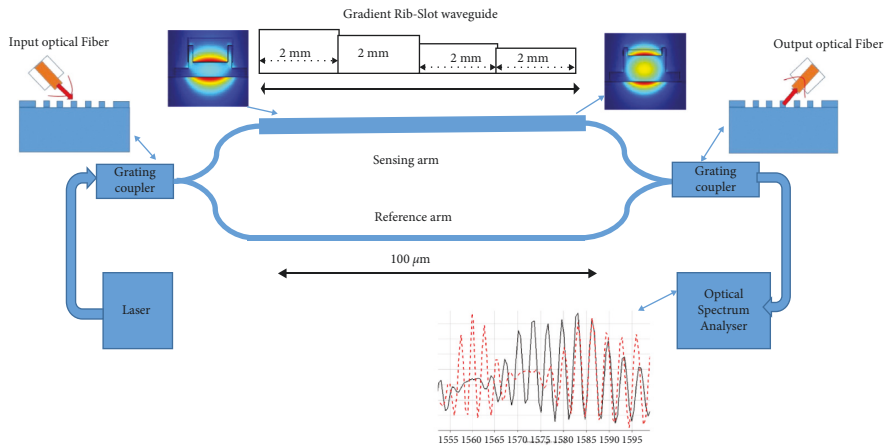

Figure 1: Silicon nitride biosensor setup with MZI and a grating coupler.

In this article, we analyzed the silicon nitride MZI sensor architecture for cancer cell detection using gradient rib and gradient rib-slot waveguide, as shown in Figure 1 [18, 21]. We use cancer cell blood samples as bulk solution for sensing. For bulk sensitivity, the interferometer-based sensor offers a high sensitivity in the range of 10-7 to 10-8 RIU [22]. By integrating the polydimethylsiloxane (PDMS) microfluidic channel in the sensor, architecture decreases the waveguide bulk sensitivity ($S_{w,\text{bulk}}$) and device sensitivity (S_d) due to leakage of molecules at edges [23]. As evanescent field decays linearly over the length of the waveguide and to avoid antibody diffusion on the surface, we propose gradient step for every 2 mm length. The response of the gradient rib waveguide over the normal cell and cancer cell in the transmission spectrum is minimal, and $S_{w,\text{bulk}}$ is 0.2568 RIU/RIU.

Our objective of the design is to accommodate analytes in the photonic biosensor integrated to mobile phones, which would increase the detection rate and sensitivity; hence, we proposed the design of a novel gradient rib-slot waveguide of rib width 970 nm, slot width 790 nm, and thickness 400 nm. This optimized structure holds the analyte without any external PDMS material and allows the sensor to be integrated with mobile phones in future. This structure also enhances the analyte transportation more effective. This results in increased interaction of analytes with light and exhibits more number of peaks in the transmission spectrum compared with the gradient-rib waveguide. The waveguide bulk sensitivity ($S_{w,\text{bulk}}$) and device sensitivity (S_d) were found to be 2.0699 RIU/RIU and 568 nm/RIU through finite-difference time-domain (FDTD) analysis. These results were obtained for cancer cells, and this approach may be extended to other generic biomolecules of different sizes and refractive indices.

2. Materials and Methods

In this section, basic components of the photonic waveguide biosensor and properties of MZI with two different types of waveguide geometry structures are presented.

2.1. Properties of the Proposed Silicon Nitride (Si3N4) Photonic Waveguide Biosensor. Silicon nitride offers broad biosensing applications for integrated point-of-care devices. The operating wavelength of silicon nitride ranges from 400 nm to 3.7 μm [18], which provides scope for designing instant-sensing biophotonic chip that can be integrated to mobile phones in future. In the asymmetric Mach–Zehnder interferometer configuration, the rib and novel rib-slot waveguide are used as the sensing arm. The other waveguide sensing structures are strip [24, 25], slot [26], double-slot [27], and sub-wavelength grating [28, 29] for biosensing applications to detect various diseases. The interferometer sensor gives high sensitivity (10-7 to 10-8 RIU), and it can operate at a telecommunication wavelength. Optimization of MZI improves the sensitivity of the sensor based on the evanescent field absorption over the waveguide structure. The design of the waveguide structure is different depending on the concentration of the sample used [30]. To increase the interaction of the evanescent field over the sensing arm, the proposed design of the novel gradient rib-slot waveguide structure has a sensing window of length 8 mm with an analyte volume of 1.0476×10^{-6} mm^3. In FDTD simulation, each gradient step length of 2 mm has different analyte thicknesses ranging from 400 nm to 90 nm. Our earlier study [31] showed that the sensitivity of the silicon nitride waveguide structure is better than the silicon waveguide structure. Better absorption in the transmission spectrum leads to detect a particular biomolecule present in the sample. The transmission loss in the waveguide depends on the absorption of photons by the sample in the cladding region. In most commonly used 450 nm width wire waveguide, the loss ranges from 2.5 dB to 3.5 dB. The roughness of the sidewalls can significantly influence the propagation loss. In addition, when the rib waveguide is immersed in water, the intrinsic loss will decrease. Thus, the confinement factor of the rib waveguide is smaller, but it is more tolerant to fabrication process errors due to waveguide width variation. Sidewall roughness in the wire waveguide is vital for evanescent sensing. Rib waveguides are preferred for evanescent sensing because sidewall roughness has less effect on them [16].

2.2. Analysis for Cancer Cell Detection. Every disease blood cell sample has a different range in refractive index, and the blood sample of a healthy person is 1.35 [32].

The light propagation in MZI waveguide will be varied due to the refractive index of cancer cells with the analyte thickness of 400 nm, 250 nm, 150 nm, and 90 nm. In the waveguide simulation, the refractive index of the cancer cells is applied over the surface of the sensing arm of MZI [22], and the corresponding variation in the transmission spectrum of cancer cell and healthy blood sample at 1550 nm is observed by using Optical Spectrum Analyzer.

2.3. Sensor Performance Evaluation by Sensitivity. FDTD accurately simulates the physical activity of photonics and optoelectronic circuits and systems. Analysis of electromagnetic wave propagation in the photonic device was performed by the FDTD approach. Due to this, computational electromagnetics has become an important area of research in developing efficient sensing platforms. In the waveguide structure, the mode profile overlaps with analytes highly. The change in effective index (neff) and refractive index of analyte (nc) can be in measurable quantity as bulk sensitivity [33].

The waveguide bulk sensitivity novel gradient strip-slot waveguide equation is as follows:

$$S_{w,\text{bulk}} = \frac{\partial n_{\text{eff}}}{\partial n_c} \frac{\text{RIU}}{\text{RIU}}. \quad (1)$$

Architecture (MZI) bulk sensitivity $S_{a\,(\text{MZI}),\text{bulk}}$ equation for the novel gradient strip-slot waveguide with (λ_r) shift in resonance wavelength is as follows:

$$S_{a\,(\text{MZI}),\text{bulk}} = \frac{\partial \lambda_r}{\partial n_{\text{eff}}} \frac{\text{nm}}{\text{RIU}}. \quad (2)$$

The efficiency of this sensor is calculated by device sensitivity S_d for novel gradient strip-slot waveguide:

$$S_d = \frac{\partial \lambda_r}{\partial n_c} \frac{\text{nm}}{\text{RIU}}. \quad (3)$$

We analyzed this waveguide sensor at $\lambda 0 = 1550$ nm. To validate this sensor sensitivity with other different wavelengths, the following equation is used to calculate normalized sensitivity S_d'':

$$S_d'' = \frac{S_d}{\lambda_0}\left(\text{RIU}^{-1}\right). \quad (4)$$

3. Results and Discussion

In the silicon photonic waveguide biosensor, evanescent wave interacts with analytes surrounding the core. Transverse electric mode is irregular at sidewalls, so the intensity of light waves will be maximum at the top of the waveguide structure. In this proposed design, we analyzed rib and gradient step rib-slot waveguide to get more interaction with samples over the length of 8 mm [34, 35]. The rib waveguide structure is more suitable for biosensing applications. The transverse-electric (TE) polarization mode in the rib structure exhibits good performance over the waveguide for high index-contrast. TE mode exploits light vertically, so the analyte interaction with the waveguide has improved the bulk sensitivity. In the strip waveguide, the analyte interaction is only with the horizontal surface area. The field effect in the bottom layer comprising silicon oxide has no effect on sensitivity. At 1550 nm, the well-established CMOS foundry waveguide with a geometric width of 970 nm and height of 400 nm is used. In the proposed waveguide structure, transverse-electric field that exceeds 450 nm from the surface core provides higher sensitivity than TM [15]. This gradient-step waveguide structure helps to avoid antibody diffusion on the surface. By analysing such advantages, the proposed waveguide with 970 nm width is appropriately chosen. To obtain higher bulk sensitivity, the analyte thickness is optimized.

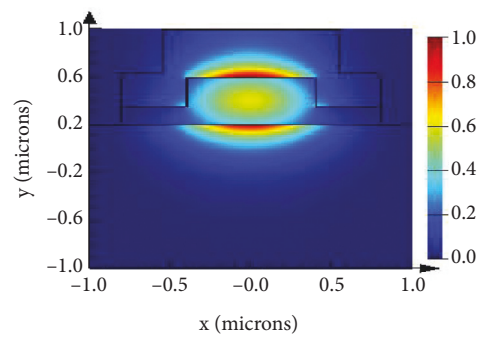

Figure 2: Rib waveguide with analyte.

3.1. Analyte Transporting for Bulk Sensitivity. The biosensor uses biological analyte placed in sensing arm where the analyte interacts with the evanescent field, which is above the core. The analyte is a biomolecule that is minimal in its concentration, so the viscosity and density of the sample are not changed. Normally, the human C-reactive protein (CRP) molecule weight is 115 kilodalton. The analyte is placed in sensing arm to obtain bulk sensitivity of the photonic waveguide sensor. The concentration of the analyte at waveguide surface $[A]_{\text{surface}}$ involves the variations of thickness and reaction of TE mode, which exceeds the waveguide surface [A] (x, y, t).

The temporal and spatial variations of the analyte in the sensing arm are described by the following diffusion equation:

$$\frac{\partial [A]}{\partial t} + u\frac{\partial [A]}{\partial x} + v\frac{\partial [A]}{\partial y} = D\left(\frac{\partial^2 [A]}{\partial x^2} + \frac{\partial^2 [A]}{\partial t^2}\right) + G, \quad (5)$$

where [A] is the analyte concentration in bulk, D is the diffusion coefficient of the analyte, and G denotes the reaction of the biomolecule in the waveguide surface [23]. The bulk sensitivity of the biosensor was analysed for four different analyte thicknesses, viz., 400 nm, 250 nm,150 nm, and 90 nm, in the waveguide. In the rib and rib-slot waveguide structure, the effective index of each analyte thickness of the different samples is analyzed through FDTD [23]. Based on

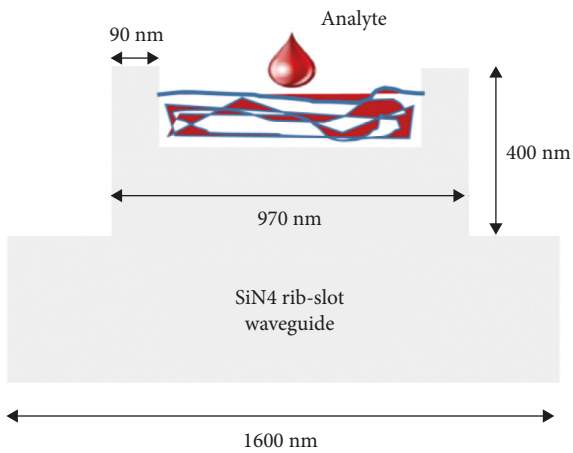

Figure 3: Novel gradient step rib-slot waveguide with analyte.

Table 1: Refractive index of different cancer cells [32].

Name of the cell	Disease	Refractive index
Normal		1.35
Jurkat	Leukemia	1.39
HeLa	Cervical cancer	1.392
PC-12	Brain	1.395
MDA-MB-231	Breast cancer	1.399
MCF-7	Breast cancer	1.401

Table 2: Analysis of rib waveguide bulk sensitivity with the analyte thickness of 400 nm to 90 nm.

RI	400 nm waveguide bulk sensitivity	250 nm waveguide bulk sensitivity	150 nm waveguide bulk sensitivity	90 nm waveguide bulk sensitivity
1.35–1.401	0.3117 RIU/RIU 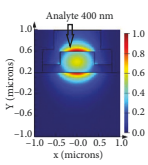	0.2501 RIU/RIU 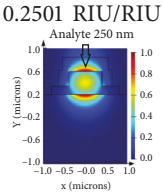	0.1882 RIU/RIU 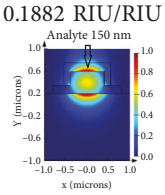	0.12764 RIU/RIU 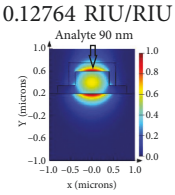

the various analyte thickness, the rib and rib-slot waveguides for normal and cancer cell are measured at 1550 nm. Lumerical INTERCONNECT has foundry-specific PDK, which verifies the fabrication feasibility of this sensor. Figure 1 shows the silicon nitride biosensor setup. MZI rib waveguide sensor and novel gradient step rib-slot waveguide sensor are shown in Figures 2 and 3, respectively.

The optimized waveguide geometry of the rib structure is 400 nm thick, and 970 nm width is analyzed for sensitivity, applying bulk solution as analyte thickness. For bulk sensitivity calculation, the refractive index of the analyte normal cell is 1.35 and of the cancer cells varies from 1.39 to 1.401, as shown in Table 1. In this process, the effective index of each thickness is calculated.

FDTD analysis of the rib waveguide with analyte thickness of 400 nm, 250 nm, 150 nm, and 90 nm was carried out. Based on the effective index, using equations (1) and (3), the bulk sensitivity for different refractive indices was computed, and the results are provided in Table 2. In this physical environment, the sensor is analysed with integration of all analyte thickness in the MZI sensing arm with a total length of 8mm. The density and viscosity of the analyte are not constant in the sensor physically. Based on these environmental factors, to improve the sensor sensitivity, the analyte thickness ranging from 400 nm to 90 nm with each thickness of the sensing arm with a length of 2 mm is analyzed.

The peak of the transmission spectrum of the rib waveguide, as shown in Figure 4, for the sample refractive index of 1.35 (normal cells) and 1.401 (cancer cells) is observed at 1563 nm wavelength. This shift in the transmission spectrum makes the sensor detect Breast Cancer (MCF-7). However, this rib waveguide structure is insensitive at 1563 nm over the normal cells. Due to this, the sensor detects cancer cells with minor variations in the transmission spectrum.

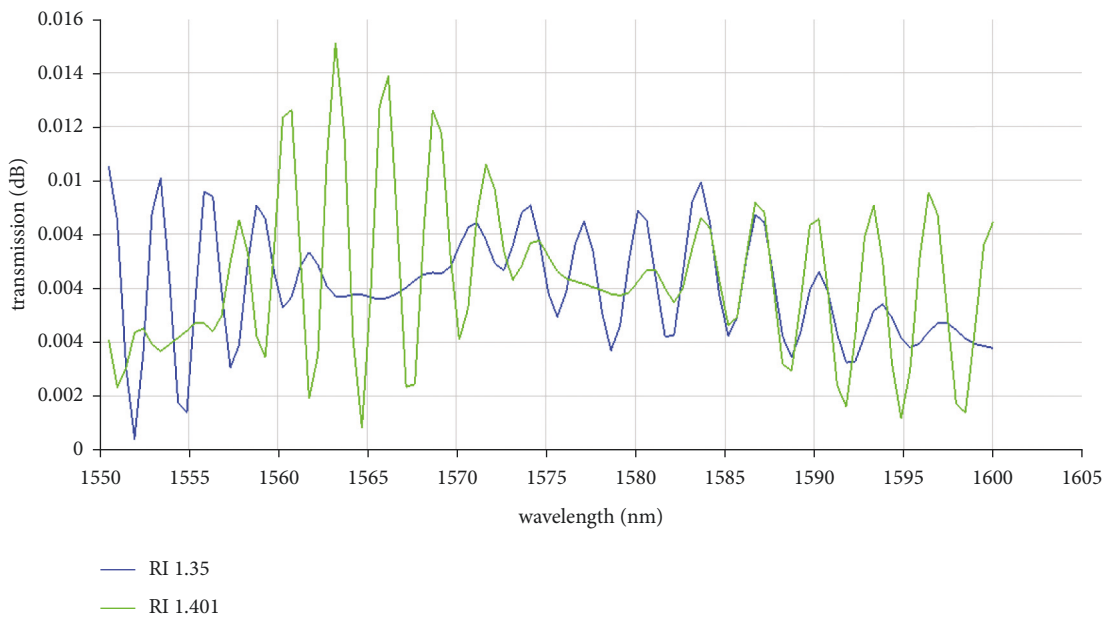

Figure 4: Transmission spectrum of normal cells with refractive index 1.35 vs Breast Cancer (MCF-7) cells with refractive index 1.401 of rib waveguide with integrated analyte thickness of 400 nm, 250 nm, 150 nm, and 90 nm.

Table 3: Analysis of bulk sensitivity of the rib-slot waveguide with 400 nm analyte thickness.

RI	Effective index	Effective area	400 nm bulk sensitivity
1.35	1.469133	1.53003	
1.39	1.479298	1.47212	
1.392	1.479832	1.46935	
1.395	1.480636	1.46522	
1.399	1.481717	1.45975	0.2574 (RIU/RIU)
1.401	1.482261	1.45703	

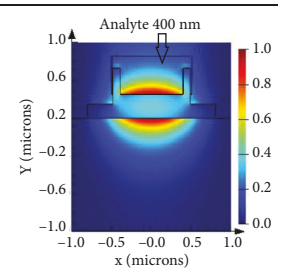

Table 4: Analysis of bulk sensitivity of rib-slot waveguide with 250 nm analyte thickness.

RI	Effective index	Effective area	250 nm bulk sensitivity
1.35	1.515538	1.26747	
1.39	1.523636	1.24779	
1.392	1.52405	1.24683	
1.395	1.524673	1.24538	
1.399	1.525507	1.24346	0.2033 (RIU/RIU)
1.401	1.525925	1.2425	

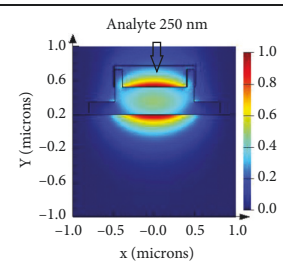

Table 5: Analysis of bulk sensitivity of rib-slot waveguide with 150 nm analyte thickness.

RI	Effective index	Effective area	150 nm bulk sensitivity
1.35	1.549438	1.16119	
1.39	1.555138	1.15424	
1.392	1.555426	1.15388	
1.395	1.555857	1.15334	
1.399	1.556433	1.15261	0.1333 (RIU/RIU)
1.401	1.556721	1.15225	

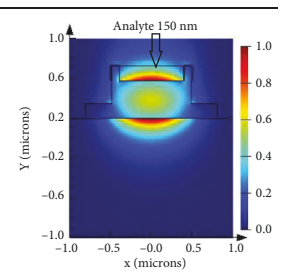

Table 6: Analysis of bulk sensitivity of rib-slot waveguide with 90 nm analyte thickness.

RI	Effective index	Effective area	90 nm bulk sensitivity
1.35	1.569833	1.11425	
1.39	1.573702	1.11248	
1.392	1.573895	1.11236	
1.395	1.574184	1.11219	
1.399	1.574569	1.11195	0.0960 (RIU/RIU)
1.401	1.574761	1.11182	

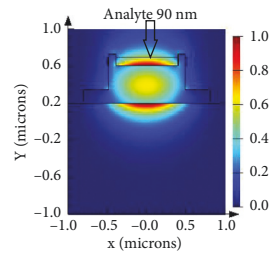

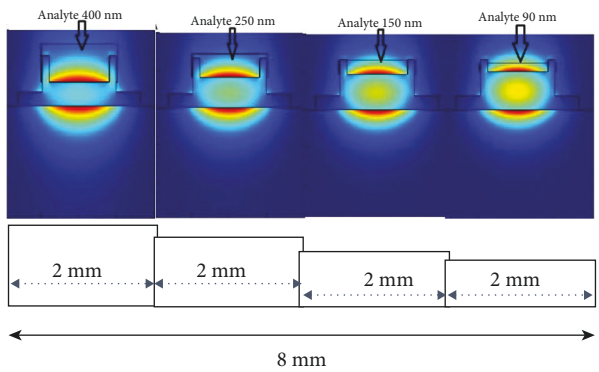

Figure 5: Gradient rib-slot waveguide structure with a width of 450 nm and height of 220 nm with integrated analyte thickness of 400 nm, 250 nm, 150 nm, and 90 nm.

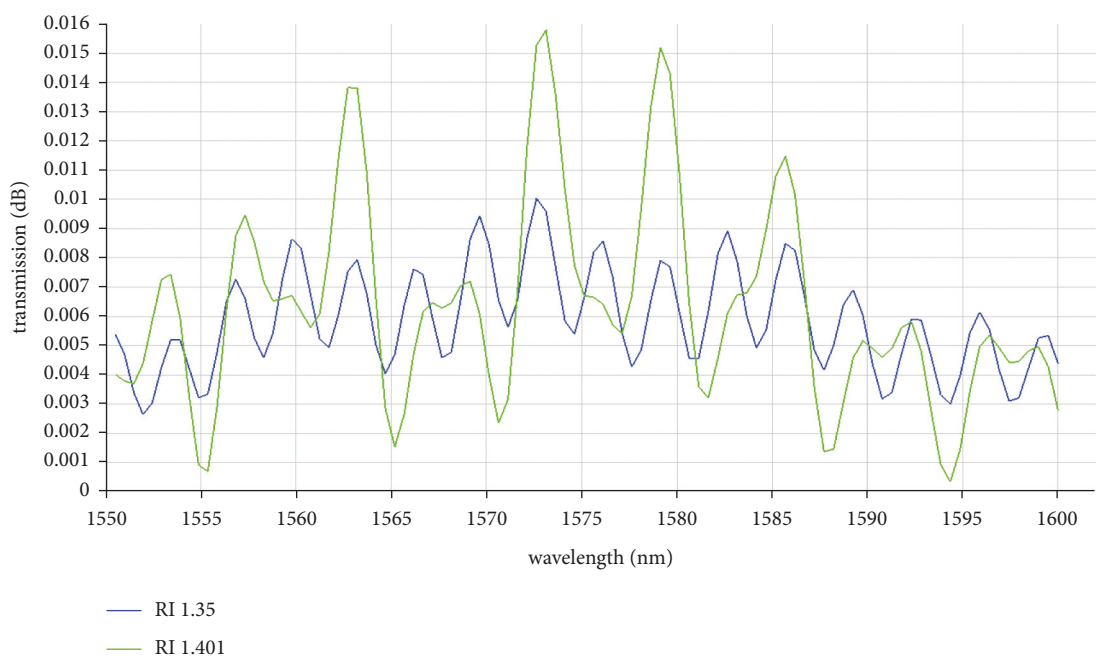

Figure 6: Silicon nitride rib-slot waveguide transmission spectrum of normal cells with refractive index 1.35 vs. Breast Cancer (MCF-7) cells with refractive index of 1.401 with integrated analyte thickness of 400 nm, 250 nm, 150 nm, and 90 nm.

3.2. Novel Gradient Step Rib-Slot Waveguide. This rib-slot waveguide with analyte is shown in Figure 3, a sensitive and enhanced guiding structure that provides a better confinement factor. Integration of the sample holder to the sensor is complex in fabrication over the small region. This proposed gradient step rib-slot waveguide holds the sample effectively without any polydimethylsiloxane (PDMS) layer. Numerically, for different analyte thickness layers, the effective area was computed for 400 nm, 250 nm, 150 nm, and 90 nm; they are tabulated in Tables 3, 4, 5, and 6, respectively, with waveguide bulk sensitivity using equation (1) and sensor architecture sensitivity using equation (2). The theoretical

Table 7: Comparison of bulk sensitivity of $\lambda 0 = 1550$ nm with other silicon-based photonic sensors.

Sensor	Architecture	$S_{w,\text{bulk}}$(RIU/RIU)	S_d (nm/RIU)	S''_d (RIU^{-1})
[38]	Ring	0.45	383	0.247
[39]	Ring	0.89	490	0.316
[28]	Ring	0.85	440	0.284
[40]	Ring	0.80	580	0.374
[41]	PSBG	n/a	579	0.374
[42]	Ring	0.97	575	0.371
[43]	Ring	1.03	545	0.352
[33]	Bragg	0.93	507	0.387
[44]	MZI	0.79	−599	−0.386
This work	MZI	**2.0699**	**568**	**0.366**

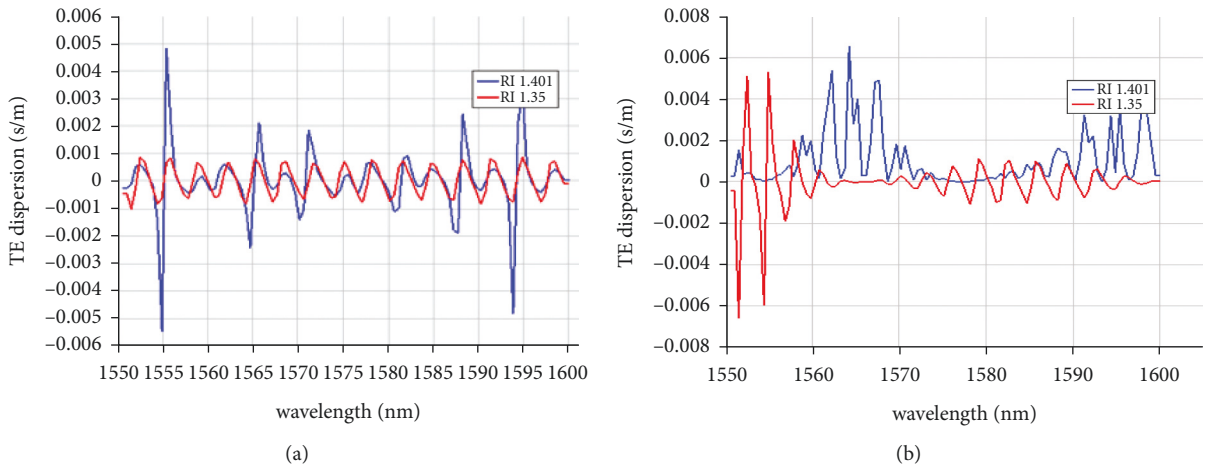

Figure 7: Dispersion of RI 1.35 normal cells and 1.401 cancer cells: (a) rib waveguide and (b) rib-slot waveguide.

analysis has been investigated considering the fabrication tolerance of the waveguide structure. The key task of waveguide optimization for bulk sensitivity is mode field distribution over the sensor surface. Analysis of the bulk sensitivity in the rib-slot waveguide, slot geometry of the 790 nm width, and 400 nm thickness with low index region that influences the analyte perfectly [36]. The gap region of the rib-slot guiding structure highly supports the TE mode, which gives evanescent waves to interact with the analyte in the highly effective area [31]. Thus, the waveguide guiding structure strongly influences the bulk sensitivity of this gradient step rib-slot biosensor. By integrating this in the Mach–Zehnder interferometer, the design of silicon photonics label-free biosensing for point-of-care devices will be more effective, and fabrication tolerance will be less compared to conventional waveguide structures like strip and slot waveguides.

By increasing the effective surface area in the sensor, the sample interacts more efficiently to obtain high waveguide bulk sensitivity. This numerical analysis of 400 nm, 250 nm, 150 nm, and 90 nm thickness in FDTD has been carried out based on device operation in the physical environment. Integration of all analyte thicknesses in the MZI sensing arm with a total length of 8 μm generates increased absorption at three different wavelengths in the transmission spectrum, as shown in Figure 5. This proposed rib-slot waveguide geometry optimization increases the detection rate of cancer cells compared with single analyte thickness of sensing arm length two μm waveguide.

The transmission spectrum of the rib-slot waveguide in Figure 6 shows the peaks at three different points of wavelength, 1563 nm, 1573 nm, and 1579 nm, of the sensor to detect Breast Cancer (MCF-7) cells. However, the rib-slot waveguide structure provides a good response and differentiates the cancer cells from the normal human cells. From the numerical analysis of different geometric, the proposed design of novel gradient rib-slot waveguide structure is in high bulk sensitivity. With 90 nm analyte thickness, in Table 7, the bulk sensitivity of breast cancer cells (MCF-7) is 1.1240 (RIU/RIU), which is higher than that in the rib waveguide. This structure makes the sensor efficient in detecting cancer cells. This design can be integrated in a point-of-care sensor system with a read-out.

The performance of the sensor depends upon the TE polarization on waveguide mode, as this analyte thickness is more sensitive to refractive index changes in cladding. In this numerical analysis, two different waveguide geometry structures, rib and rib-slot, have been simulated and the dispersion characteristics are studied [37]. In convention, silicon nitride waveguides achieve sharp bending with low loss, as shown in Figure 7(b), dispersion due to modes that overlap with the analyte. Rib-slot waveguide is more

dispersive than rib waveguide, as shown in Figure 7(a). However, the sensitivity of the rib-slot waveguide sensor is higher. Normalized sensitivity S_d'' will be calculated to compare ($\lambda 0$) for different wavelengths using equation (4).

4. Conclusion

We proposed silicon nitride MZI sensor architecture as integrated biosensor for point-of-care device. This biosensor detects virus and biomolecules fast and is cost-effective. Our simulated analysis determines optimized waveguide geometry that maximizes the bulk sensitivity. MZI utilizes the refractive index of different cancer cells (1.39–1.401) to determine the waveguide bulk sensitivity ($S_{w,\text{bulk}}$). In addition, we compared gradient step rib waveguide with rib-slot waveguide. The results show that the gradient step rib-slot waveguide is efficient and can hold analytes without any PDMS material. Analyte transportation and leakage of molecules at the edge of the waveguide lead to decrease in the sensitivity of the sensor. Our proposed design exhibits a high ($S_{w,\text{bulk}}$) of 2.0699 RIU/RIU and a device sensitivity (S_d) of 568 nm/RIU calculated based on analyte thickness. The absorption of cancer cells at three wavelengths 1563 nm, 1573 nm, and 1579 nm offers high detection rate compared with the standard rib waveguide. The silicon nitride-based waveguide biosensor may be fabricated using CMOS E-beam lithography, and its stability will be matched to the simulated results. The proposed biosensor can provide test results in a short time than the conventional biopsy, which takes two days to detect cancer cells.

Data Availability

The data underlying the results presented in this paper are not publicly available at this time but may be obtained from the authors upon reasonable request.

Conflicts of Interest

The authors declare that there are no conflicts of interest.

Authors' Contributions

Design and simulation analysis were performed by Prasanna Kumaar. The manuscript preparation was performed by Prasanna Kumaar and Sivasubramanian.

Acknowledgments

This proposed work was performed in the Fiber Optics Laboratory on Lumerical software provided by Vellore Institute of Technology, Chennai.

References

[1] N. Bhalla, Y. Pan, Z. Yang, and A. F. Payam, "Opportunities and challenges for biosensors and nanoscale Analytical tools for pandemics: COVID-19," *ACS Nano*, vol. 14, no. 7, pp. 7783–7807, Jul. 2020.

[2] "The global challenge of cancer," *Naturaliste Canadien*, vol. 1, no. 1, pp. 1-2, 2020.

[3] H. Sung, J. Ferlay, R. L. Siegel et al., "Global cancer statistics 2020: GLOBOCAN estimates of incidence and mortality worldwide for 36 cancers in 185 countries," *CA: A Cancer Journal for Clinicians*, vol. 71, no. 3, pp. 209–249, 2021.

[4] B. Hayes, C. Murphy, A. Crawley, and R. O'Kennedy, "Developments in point-of-care diagnostic Technology for cancer detection," *Diagnostics*, vol. 8, no. 2, p. 39, 2018.

[5] S. Parra, E. Carranza, J. Coole et al., "Development of low-cost point-of-care technologies for cervical cancer prevention based on a single-board computer," *IEEE Journal of Translational Engineering in Health and Medicine*, vol. 8, pp. 1–10, 2020.

[6] S. Schultz, D. R. Smith, J. J. Mock, and D. A. Schultz, "Single-target molecule detection with nonbleaching multicolor optical immunolabels," in *Proceedings of the National Academy of Sciences*, vol. 97, no. 3, pp. 996–1001, California, CA, USA, February 2000.

[7] A. Cassedy, A. Parle-McDermott, and R. O'Kennedy, "Virus detection: a review of the current and emerging molecular and immunological methods," *Frontiers in Molecular Biosciences*, vol. 8, 2021.

[8] V. Naresh and N. Lee, "A review on biosensors and recent development of nanostructured materials-enabled biosensors," *Sensors*, vol. 21, no. 4, p. 1109, 2021.

[9] Y. Du, H. Wang, W. Cui et al., "Foodborne disease risk prediction using multigraph structural long short-term memory networks: algorithm design and validation study," *JMIR Medical Informatics*, vol. 9, no. 8, Article ID e29433, 2021.

[10] F. Deeba, S. Kun, F. Ali Dharejo, and Y. Zhou, "Sparse representation based computed tomography images reconstruction by coupled dictionary learning algorithm," *IET Image Processing*, vol. 14, no. 11, pp. 2365–2375, 2020.

[11] C. Chen and J. Wang, "Optical biosensors: an exhaustive and comprehensive review," *Analyst*, vol. 145, no. 5, pp. 1605–1628, 2020.

[12] J. Yoon, M. Shin, T. Lee, and J.-W. Choi, "Highly sensitive biosensors based on biomolecules and functional nanomaterials depending on the types of nanomaterials: a perspective review," *Materials*, vol. 13, no. 2, p. 299, 2020.

[13] Y. Liu, Q. Liu, S. Chen, F. Cheng, H. Wang, and W. Peng, "Surface plasmon resonance biosensor based on smart phone platforms," *Scientific Reports*, vol. 5, no. 1, Article ID 12864, 2015.

[14] D. Thomson, A. Zilkie, J. E. Bowers et al., "Roadmap on silicon photonics," *Journal of Optics*, vol. 18, no. 7, 2016.

[15] J. Milvich, D. Kohler, W. Freude, and C. Koos, "Surface sensing with integrated optical waveguides: a design guideline," *Optics Express*, vol. 26, no. 16, Article ID 19885, 2018.

[16] L. Ali, M. U. Mohammed, M. Khan, A. H. B. Yousuf, and M. H. Chowdhury, "High-quality optical ring resonator-based biosensor for cancer detection," *IEEE Sensors Journal*, vol. 20, no. 4, pp. 1867–1875, 2020.

[17] A. Densmore, E. Post, D.-X. Xu et al., "A silicon-on-insulator photonic wire based evanescent field sensor," *IEEE Photonics Technology Letters*, vol. 18, no. 23, pp. 2520–2522, 2006.

[18] R. Baets, A. Z. Subramanian, S. Clemmen et al., "Silicon photonics: silicon nitride versus silicon-on-insulator," in *Proceedings of the Optical Fiber Communication Conference*, Washington D.C., USA, 2016.

[19] D. J. Blumenthal, R. Heideman, D. Geuzebroek, A. Leinse, and C. Roeloffzen, "Silicon nitride in silicon photonics," in *Proceedings of the IEEE*, vol. 106, no. 12, pp. 2209–2231, Piscataway, NJ, USA, December 2018.

[20] Y. Xie, M. Zhang, and D. Dai, "Design rule of mach-zehnder interferometer sensors for ultra-high sensitivity," *Sensors*, vol. 20, no. 9, p. 2640, 2020.

[21] A. Z. Subramanian, E. Ryckeboer, A. Dhakal et al., "Silicon and silicon nitride photonic circuits for spectroscopic sensing on-a-chip (Invited)," *Photonics Research*, vol. 3, no. 5, p. B47, 2015.

[22] C. Chen, X. Hou, and J. Si, "Protein analysis by Mach-Zehnder interferometers with a hybrid plasmonic waveguide with nano-slots," *Optics Express*, vol. 25, no. 25, Article ID 31294, 2017.

[23] M. Selmi, M. H. Gazzah, and H. Belmabrouk, "Optimization of microfluidic biosensor efficiency by means of fluid flow engineering," *Scientific Reports*, vol. 7, no. 1, p. 5721, 2017.

[24] S. Prasanna Kumaar and A. Sivasubramanian, "Optimization of silicon photonic strip waveguide for detection of diabetes mellitus," *Materials Today: Proceedings*, vol. 45, 2020.

[25] P. Muñoz, G. Micó, L. Bru et al., "Silicon nitride photonic integration platforms for visible, near-infrared and mid-infrared applications," *Sensors*, vol. 17, no. 9, pp. 2088–2125, 2017.

[26] R. R. Singh, S. Kumari, A. Gautam, and V. Priye, "Glucose sensing using slot waveguide-based SOI ring resonator," *IEEE Journal of Selected Topics in Quantum Electronics*, vol. 25, no. 1, pp. 1–8, 2019.

[27] X. Sun, D. Dai, L. Thylén, and L. Wosinski, "High-sensitivity liquid refractive-index sensor based on a Mach-Zehnder interferometer with a double-slot hybrid plasmonic waveguide," *Optics Express*, vol. 23, no. 20, Article ID 25688, 2015.

[28] H. Yan, L. Huang, X. Xu et al., "Unique surface sensing property and enhanced sensitivity in microring resonator biosensors based on subwavelength grating waveguides," *Optics Express*, vol. 24, no. 26, Article ID 29724, 2016.

[29] J. Gonzalo Wangüemert-Pérez, P. Cheben, A. Ortega-Moñux et al., "Evanescent field waveguide sensing with subwavelength grating structures in silicon-on-insulator," *Optics Letters*, vol. 39, no. 15, p. 4442, 2014.

[30] Q. Liu, X. Tu, K. W. Kim et al., "Highly sensitive Mach-Zehnder interferometer biosensor based on silicon nitride slot waveguide," *Sensors and Actuators B: Chemical*, vol. 188, pp. 681–688, 2013.

[31] S. Prasanna Kumaar and A. Sivasubramanian, "Optimization of the transverse electric photonic strip waveguide biosensor for detecting diabetes mellitus from bulk sensitivity," *Journal of Healthcare Engineering*, vol. 2021, Article ID 6081570, 8 pages, 2021.

[32] X. J. Liang, A. Q. Liu, X. M. Zhang, P. H. Yap, T. C. Ayi, and H. S. Yoon, "Determination of refractive index for single living cell using integrated biochip," in *Proceedings of the 13th International Conference on Solid-State Sensors, Actuators and Microsystems, 2005. Digest of Technical Papers. TRANSDUCERS'05*, vol. 2, pp. 1712–1715, Seoul, Korea (South), June 2005.

[33] C. Pérez-Armenta, A. Ortega-Moñux, J. Čtyroký et al., "Narrowband Bragg filters based on subwavelength grating waveguides for silicon photonic sensing," *Optics Express*, vol. 28, no. 25, Article ID 37971, 2020.

[34] V. R. Almeida, Q. Xu, C. A. Barrios, and M. Lipson, "Guiding and confining light in void nanostructure," *Optics Letters*, vol. 29, no. 11, p. 1209, 2004.

[35] T. Claes, J. G. Molera, K. De Vos, E. Schacht, R. Baets, and P. Bienstman, "Label-free biosensing with a slot-waveguide-based ring resonator in silicon on insulator," *IEEE Photonics Journal*, vol. 1, no. 3, pp. 197–204, 2009.

[36] A. Habibzadeh-Sharif and M. Soleimani, "Rib-based slot waveguide for nonlinear silicon photonics," in *Proceedings of the 20th Iranian Conference on Electrical Engineering*, pp. 55–60, Tehran, Iran, May 2012.

[37] S. Chandran, R. K. Gupta, and B. K. Das, "Dispersion enhanced critically coupled ring resonator for wide range refractive index sensing," *IEEE Journal of Selected Topics in Quantum Electronics*, vol. 23, no. 2, pp. 424–432, 2017.

[38] V. Donzella, A. Sherwali, J. Flueckiger, S. M. Grist, S. T. Fard, and L. Chrostowski, "Design and fabrication of SOI microring resonators based on sub-wavelength grating waveguides," *Optics Express*, vol. 23, no. 4, p. 4791, 2015.

[39] J. Flueckiger, S. Schmidt, V. Donzella et al., "Sub-wavelength grating for enhanced ring resonator biosensor," *Optics Express*, vol. 24, no. 14, Article ID 15672, 2016.

[40] E. Luan, H. Yun, L. Laplatine et al., "Enhanced sensitivity of subwavelength multibox waveguide microring resonator label-free biosensors," *IEEE Journal of Selected Topics in Quantum Electronics*, vol. 25, no. 3, pp. 1–11, 2019.

[41] E. Luan, H. Yun, M. Ma, D. M. Ratner, K. C. Cheung, and L. Chrostowski, "Label-free biosensing with a multi-box subwavelength phase-shifted bragg grating waveguide," *Biomedical Optics Express*, vol. 10, no. 9, p. 4825, 2019.

[42] E. Luan, K. M. Awan, K. C. Cheung, and L. Chrostowski, "High-performance sub-wavelength grating-based resonator sensors with substrate overetch," *Optics Letters*, vol. 44, no. 24, p. 5981, 2019.

[43] C.-W. Chang, X. Xu, S. Chakravarty et al., "Pedestal subwavelength grating metamaterial waveguide ring resonator for ultra-sensitive label-free biosensing," *Biosensors and Bioelectronics*, vol. 141, Article ID 111396, 2019.

[44] M. Odeh, K. Twayana, K. Sloyan, J. E. Villegas, S. Chandran, and M. S. Dahlem, "Mode sensitivity analysis of subwavelength grating slot waveguides," *IEEE Photonics Journal*, vol. 11, no. 5, pp. 1–10, 2019.

Hindawi
International Journal of Optics
Volume 2022, Article ID 7883851, 9 pages
https://doi.org/10.1155/2022/7883851

Research Article

Nonlinear Extended Kalman Filter for Attitude Estimation of the Fixed-Wing UAV

Tang Xiaoqian,[1] Zhao Feicheng,[2] Tang Zhengbing,[1] and Wang Hongying[3]

[1]*Xi'an Aeronautical University, School of Electronic Engineering, Xi'an, China*
[2]*National Aviation University, Kyiv, Ukraine*
[3]*Sinohydro Bureau 3Co., Ltd, Xi'an, China*

Correspondence should be addressed to Tang Xiaoqian; tangxiaoqian83@163.com

Received 29 October 2021; Accepted 4 January 2022; Published 1 February 2022

Academic Editor: Bhagwan Das

Flying vehicle's navigation, direction, and control in real-time results in the design of a strap-down inertial navigation system (INS). The strategy results in low accuracy, performance with correctness. Aiming at the attitude estimation problem, many data fusion or filtering methods had been applied, which fail in many cases, which attains the nonlinear measurement model, process dynamics, and high navigation range. The main problem in unmanned aerial vehicles (UAVs) and flying vehicles is the determination of attitude angles. A novel attitude estimation algorithm is proposed in this study for the unmanned aerial vehicle (UAV). This research article designs two filtering algorithms for fixed-wing UAVs which are nonlinear for the attitude estimation. The filters are based on Kalman filters. The unscented Kalman filter (UKF) and cubature Kalman filter (CKF) were designed with different parameterizations of attitude, i.e., Euler angle (EA) and INS/unit quaternion (UQ) simultaneously. These filters, EA-UKF and INS-CKF, use the nonlinear process and measurement model. The computational results show that among both filters, the CKF attains a high accuracy, robustness, and estimation for the attitude estimation of the fixed-wing UAV.

1. Introduction

The unmanned aerial vehicle (UAV) becomes an exploration hotspot recently in the area of robotics [1]. Similarly, microvehicles attain a lot of concentration due to their small sizes, lower risk, and easy application. The objectivity of the UAV is tested in low altitudes due to the shadowing of GPS signals [2]. Flying vehicles show great interest in the military and civilian sectors. Different types of missions are accomplished with UAVs such as tracking, inspection, searching, mapping, and much more. Recently, the advances in the tracking feature decreases the size as well as the cost of the camera [3, 4]. A navigation system is widely used in the navigation of autonomous robots and for mapping. These robots or vehicles are equipped with a camera for navigation in a GPS environment. Mostly, the strap-down inertial navigation system (SINS) occupies an electromechanical system (EMS) that attains low cost and consumption of power. The performance and robustness of EMS based on the INS improve due to nonlinear filtering, which helps in attaining attitude estimation and tracking of the UAV [5]. The information of attitude and position is attained by the INS with abundant update rate, and information combination is the way to increase the accuracy. The INS attains the capability to estimate the pose of the camera using the Kalman filter (KF) where the navigation measurement system is for visual measurement and update [6–8]. On the other hand, growing interest has been seen in using nonlinear filtering methods for attitude estimation of flying vehicles. The missions of UAVs need nonlinear dynamics, filters initialization, and estimators. Even the design of the vehicle is conservative. The most important task for UAVs is attitude estimation. Flying vehicles becomes cheaper and reliable due to the growing range of applications in UAVs. It also develops an interest in designing simple and robust algorithms for the attitude estimation of flying vehicles.

In reference to [9], the UKF is proposed for the flight of the UAV. The state equation model is based on the attitude

angle differential equation formed by the fusion algorithm. The EKF helps in measuring the data of the gyro, accelerometer, and magnetometer. Static and dynamic experiments show the effectiveness of the algorithm. Experimental results show that the proposed scheme is accurate and effective. Similarly, in [10], the study proposes the attitude heading reference algorithm based on the cubature Kalman filter (CKF) for low precision of AHRS. This filter also helps in solving the nonlocal sampling problem. In the interim, the adaptive estimation algorithm realizes the estimation of motion acceleration. The simulation results show that the proposed algorithm accurately estimates the attitude and acceleration. In [11], the study proposes the low-computational complexity filter for attitude estimation of the UAV, namely, the square root UKF filter based on the KF. The basic equations of the KF are modified just because the feature of the filter is dignified. This research article bespoke to the quadrotor UAV to attain the quaternion-based model. The simulation results verify the effectiveness of the proposed algorithm. In reference to [12], an efficient approach is proposed based on the Kalman filter. The purpose of the KF is to provide the possible region in which tracking objects might occur. It will also help in reducing the computational complexity. The performance of the proposed scheme is compared with other schemes. The results reveal that the scheme attains the best performance and accuracy. Last, in another study [9] for the error of the attitude estimation algorithm, a UAV attitude estimation algorithm based on the UKF is proposed. The Euler angle method defines the attitude algorithm model of a vehicle. Similarly, the system state equation is developed. The filter algorithm helps in achieving the attitude angle of the aircraft. The simulation results show that the proposed algorithm attains a high improvement in accuracy and reliability as compared to the EKF.

The contribution of this research article is to design the two nonlinear improved Kalman filters (NIKF) to approximate the attitude of fixed-wing UAVs based on the INS. The study designs the unscented Kalman filter (UKF) and cubature Kalman filter (CKF) with the help of two different types of parameterizations/based on the Euler angle (EA) and inertial navigation system (INS). Both filters attain a nonlinear process. Then, these filters result in two different orientations, namely, EA-UKF and INS/UQ-CKF. Last, the computational simulations define the reliability, performance, and fitness of both filters.

The study is planned as follows. The introduction is presented in Section 1. The problem definition and its proposed solution are defined in Section 2. The state of art is defined in Section 3. Section 4 defines the designing of a nonlinear Kalman filter. In Section 5, attitude parameterization and estimation are presented. The simulations are done in Section 6. Section 7 presents the conclusion of this study.

2. Problem Definition and Proposed Solution

This section defines the problem statement and the proposed solution in this study. Recently, a growing interest takes place in the use of nonlinear filtering methods for the attitude estimation of UAVs. The missions assigned to flying vehicles involve the usage of nonlinear dynamics and filters initialization, and even the design of the vehicle is conservative [13, 14]. The design of the INS results in a high error, low accuracy, and performance. The main problem during the flight mission is the determination of angles. This also involves the estimation and compensation of errors. Many filters applied to attitude estimation fail due to highly nonlinear dynamics and long-range system of navigation [15]. To solve the abovementioned problems, the two nonlinear filters are designed, i.e., EA-IUKF and INS-CKF. The proposed scheme also solves the both estimation and compensation of attitude errors. The scheme creates an efficient strategy with the help of parameters and different variables to reflect the current situation. It aims towards the better performance of UAVs during the flight mission.

3. State of the Art

This section defines the recent trends in this field. In reference to [16], sensors take place for the attitude estimation of flying vehicles. The study aims towards the flying problem due to the high rate of precision. To solve this issue, the study proposed the algorithm using the Kalman filters. The algorithm attains the capability of providing high attitude estimation. The computational simulations show that Kalman filters are a highly suitable method for attitude estimation. In the study by Odry et al. [17], a fuzzy adaptive Kalman filter (FAKF) for the attitude estimation of mobile vehicles was proposed. The structure of the filter includes the EKF and FAKF to calculate the vibration of the system, acceleration, and distortions. Filter performance is evaluated with the help of a test bench. The optimization performs the tuning of filter parameters. The simulations results show the effectiveness of the proposed scheme. Similarly, in [18], the study proposes positioning technology. The architecture of the system attains the multisensor technology established on the unscented Kalman filter (UKF). It avoids the high order relationships of nonlinear equations. Last, the HIL platform helps in performing the simulations which verify the effectiveness and improves the accuracy. In reference to [19], the study design of the CKF is based on fast Euler attitude and heading reference for flying vehicles smaller in size. The abovementioned article aims to derivate the low-cost model mutual with quaternion attitude determination. It also uses fast Euler to accurate the attitude update by which the real-time solution increases. Additionally, the proposed scheme improves the overall accuracy of the filter. The simulation results demonstrate that the algorithm attains an excellent attitude solution in highly dynamic conditions. In [20, 21], the studies present the target motion estimation solution using the unmanned aerial vehicle (UAV). The UAV guidance law helps in solving the estimation problem mentioned in this manuscript. The designed estimator helps in tracking the moving ground target and provides the optimal solution in real-time. This study designs the Kalman filtering method based on inverse kinematics. The numerical simulations verify the accuracy and feasibility of the designed scheme. The simulation results show the stability in

position and velocity. Last, in [22], the study design is on the attitude estimation algorithm based on the complementary extended Kalman filter (CEKF). The inertial measurement unit (IMU) helps in deriving the attitude angle in real-time. The filtering algorithms eliminate the noise errors thereby improving the accuracy of the attitude solution. The proposed scheme is verified on MATLAB simulation. The computational results verify the effectiveness, accuracy, and robustness of the algorithm.

4. Designing of the Nonlinear Kalman Filter (NLKF)

The NLKF is a state space-based algorithm based on two phases. To calculate the state of the system, model information and measurement information are combined [23, 24].

4.1. Phase 1: Prediction. In this phase, the filter generates the prediction of system state vector $x\varepsilon R^n$ at time $t+1$. The error covariance matrix is denoted by $E\varepsilon R^{n\times n}$ and is shown in the following equation at time t.

$$\begin{cases} \hat{x}(t+1|t) = F(\hat{x}(t|t), u(t), w(t)), \\ E(t+1|t) = F(t)E(t,t)F^T(t) + K(t)Q(t)K^T(t), \\ y(t+1) = h(\hat{x}(t+1|t), v(t+1)), \end{cases} \tag{1}$$

where the estimation of the exact system state is denoted by $\hat{x}$, $F(t)$ is the process model matrix, u is a control vector, w denotes the process noise, $K(t)$ is a process noise model matrix, and v is the observation noise. The process noise is denoted by Q. The matrix E should verify the following condition.

$$E(t+1) - \operatorname{cov}[x(t+1|t) - \hat{x}(t+1|t)] \geq 0. \tag{2}$$

4.2. Phase 2: Estimate Correction. In this phase, the observation model refined the prediction/estimate produced in phase 1. Matrix $E(t)$ is improved with a lower level of uncertainties. They are calculated as

$$\begin{cases} \hat{x}(t+1|t+1) = \hat{x}(t+1|t) + L(t+1)\hat{e}(t+1), \\ E(t+1|t+1) = (I - L(t+1)H(t+1)E(t+1,t)), \end{cases} \tag{3}$$

where $\hat{e}(t+1)$ is the innovation, and the Kalman gain matrix $L(t+1)$ is given as follows:

$$\begin{cases} \hat{e}(t+1) = [y(t+1) - H(t+1)\hat{x}(t+1|t)], \\ L(t+1) = E(t+1|t)H^T(t+1)A^{-1}(t+1), \\ A(t+1) = \left[H(t+1)E(k+1|k)H^T(t+1) + M(t+1)R(t+1)M^T(t+1)\right], \end{cases} \tag{4}$$

where $H(t+1)$ is the observation model matrix, the measurement noise model matrix is M, and R is the covariance matrix of Gaussian white noise. Similarly, $F(t), K(t)$, and $H(t)$ are the Jacobian matrices. y vector contains the measurement attained by the summing system and residual reflects among the actual measurement [23].

5. Attitude Parameterization and Estimation of the UAV

5.1. Parameterization of Euler Angle (EA). In moving body axes frame, the flying airframe orientation and position cannot be described. So, a fixed inertial axes system is used to conclude the angular velocities of the airframe. Figure 1 shows the body frame and navigation frame. Three sequential rotations are used to define the orientation of an airframe concerning fixed inertial reference. The most important is the directive of rotation in EA.

In the reference frame, the relationship between the angular velocities and EA of the flight is given by

$$\begin{cases} p = \dot{\varphi} - s\theta\dot{\psi}, \\ q = c\varphi\dot{\theta} + s\varphi c\theta\dot{\psi}, \\ r = -s\varphi\dot{\varphi} + c\varphi c\theta\dot{\psi}, \end{cases} \tag{5}$$

where $c = \cos$ and $s = \sin$. The rotation angles are denoted by φ, θ, ψ, i.e., roll, pitch, and yaw, respectively. Similarly, the angular rates are denoted by p, q, and r. By assimilating the following equations, the orientation of the airframe is obtained, where $t = \tan$. In the matrix form, it can be rewritten as

$$\begin{Bmatrix} \dot{\varphi} \\ \dot{\theta} \\ \dot{\psi} \end{Bmatrix} = \begin{bmatrix} 1 & s\varphi t\theta & c\varphi t\theta \\ 0 & c\varphi & -\sin\varphi \\ 0 & \dfrac{s\varphi}{c\theta} & \dfrac{c\varphi}{c\theta} \end{bmatrix} \begin{Bmatrix} p \\ q \\ r \end{Bmatrix}. \tag{6}$$

The nonlinear filters attain effective results when designed with the base of EA. It helps in making smooth flight paths.

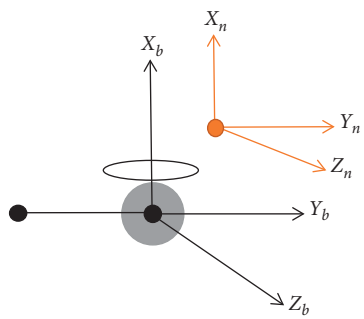

Figure 1: Body frame (b) and navigation frame (n) [24].

5.2. Unscented Kalman Filter (UKF) Based on EA. The UKF is articulated in the base of EA coordinates for the estimation of the airframe attitude of the UAV. In this part, the state vector is extended while including the gyros biases vector which is written as

$$\hat{g} = \left[g_p \;\; g_q \;\; g_r \right]^T. \tag{7}$$

5.2.1. Prediction. The control input vector and state vector are defined as follows:

$$\begin{aligned} u &= \omega^T \left[p \;\; q \;\; r \right]^T, \\ \hat{x} &= \left[\varphi \;\; \theta \;\; \psi \;\; g_p \;\; g_q \;\; g_r \right]^T. \end{aligned} \tag{8}$$

The roll, pitch, and yaw gyro biases are denoted by g_p, g_q, and g_r, respectively. Equation (1) can be reduced and can be rewritten as

$$\begin{cases} \hat{x}(t+1|t) = F(t)\hat{x}(t|t) + U(t)u(t) + w(t), \\ E(t+1|t) = F(t)E(t,t)F^T(t) + Q(t), \end{cases} \tag{9}$$

where F denotes the state transition matrix and U denotes the control input matrix and are given as follows:

$$\begin{aligned} F &= \begin{bmatrix} O_{3\times3} & T \\ O_{3\times3} & O_{3\times3} \end{bmatrix}, \\ G &= \begin{bmatrix} T \\ O_{3\times3} \end{bmatrix}. \end{aligned} \tag{10}$$

$K(t)$ denotes the process noise model and is assumed to be identical. Transformation matrix T coppices angular rates to EA rates which are written as follows:

$$T = \begin{bmatrix} 1 & s\varphi t\theta & c\varphi t\theta \\ 0 & c\varphi & -s\varphi \\ 0 & \dfrac{s\varphi}{c\theta} & \dfrac{c\varphi}{c\theta} \end{bmatrix}. \tag{11}$$

5.2.2. Correction. The observation model is needed to refine the estimation which is given as follows:

$$\begin{cases} \hat{x}(t+1|t+1) = (\hat{x}(t+1|t) + L(t+1)z(t+1)), \\ E(t+1|t+1) = (I - L(t+1)H(t+1))E(t+1,t), \\ z(t+1) = y(t+1) - H(t+1)\hat{x}(t+1|t). \end{cases} \tag{12}$$

The attitude of the UAV is estimated by a sensor as follows:

$$y = \left[\varphi_m \;\; \theta_m \;\; \psi_m \;\; j_p \;\; j_q \;\; j_r \right]^T,$$

$$\begin{cases} \varphi_m = -ct2\left(\dfrac{c_y}{\sqrt{c_y^2 + c_z^2}} \right), \\ \theta_m = -cs\left(\dfrac{c_y}{g} \right), \\ \psi_m = -ct2\left(\dfrac{m_y c\varphi - m_z s\varphi}{m_x c\theta + m_y s\varphi s\theta + m_z c\varphi s\theta} \right), \end{cases} \tag{13}$$

where m_x, m_y, and m_z are the earth's magnetic field component. Similarly, c_x, c_y, and c_z are the acceleration of the accelerometer along the body axes of the vehicle. The gravity vector is written as

$$g = \left[g_x \;\; g_y \;\; g_z \right]^T = \left[0 \;\; 0 \;\; -1 \right]^T. \tag{14}$$

5.3. Parametrization of the INS/UQ. The state equations of the INS are the error equations of the strap-down INS. The state variables are as follows:

$$X(t) = \left[\sigma q_0 \;\; \sigma q_1 \;\; \sigma q_2 \;\; \sigma q_3 \;\; \sigma e_n \;\; \sigma e_e \;\; \sigma e_u \;\; \sigma L \;\; \sigma l \;\; \sigma h \;\; \varrho_{jx} \;\; \varrho_{jy} \;\; \varrho_{jz} \;\; \varrho_{ox} \;\; \varrho_{oy} \;\; \varrho_{oz} \;\; \Lambda_{ox} \;\; \Lambda_{oy} \;\; \Lambda_{oz} \right]^T, \tag{15}$$

where σq denotes the quaternion error. σe_n, σe_e, and σe_u denote the error of north, east, and vertical. The longitude, latitude, and height are expressed by σL, σl, and σh, respectively. ϱ_j denotes the gyro drift error, and ϱ_o denotes the Markov gyro drift error. Similarly, Λ_o denotes the accelerometer drift. With the help of an error model and equations, a state equation can be built.

$$\begin{aligned}\sigma\dot{Q}_j^n = {} & 0.5\lambda_u Q_j^n\left(\omega_{ij}^j\right)\sigma Q_j^n - 0.5\lambda_d\omega_{in}^n\sigma Q_j^n + 0.5G\left(Q_j^n\right)\sigma\omega_{ij}^j \\ & - 0.5Y\left(Q_j^n\right)\sigma\omega_{in}^n,\end{aligned} \tag{16}$$

where $\sigma Q_j^n = \left[\ \sigma q_0\ \ \sigma q_1\ \ \sigma q_2\ \ \sigma q_3\ \right]^T$.

$$\begin{aligned}\sigma\dot{V}^n = {} & \sigma A_j^n f^j - \left(2\omega_{ie}^n + \omega_{en}^n\right)\times\sigma V^n + A_j^n\sigma f^j + V^n \\ & \times\left(2\sigma\omega_{ie}^n + \omega_{en}^n\right),\end{aligned} \tag{17}$$

where $\sigma V^n = \left[\ \sigma e_n\ \ \sigma e_e\ \ \sigma e_u\ \right]^T$.

$$\begin{bmatrix}\sigma\dot{L}\\ \sigma\dot{l}\\ \sigma\dot{h}\end{bmatrix} = \begin{bmatrix}0 & \frac{1}{h} & 0\\ \frac{sL}{h} & 0 & 0\\ 0 & 0 & 1\end{bmatrix}\begin{bmatrix}\sigma e_n\\ \sigma e_e\\ \sigma e_u\end{bmatrix} + \begin{bmatrix}0 & 0 & \frac{V^n}{h^2}\\ \frac{V^e sLtL}{h} & 0 & \frac{-V^e sL}{h^2}\\ 0 & 0 & 0\end{bmatrix}\begin{bmatrix}\sigma L\\ \sigma l\\ \sigma h\end{bmatrix},$$

$$\begin{aligned}&\dot{\varrho}_{jx} = \dot{\varrho}_{jy} = \dot{\varrho}_{jz} = 0,\\ &\dot{\varrho}_o = -\frac{1}{T_a}\varrho_o + \omega 1,\\ &\dot{\Lambda}_o = -\frac{1}{T_b}\Lambda_o + \omega 2,\end{aligned} \tag{18}$$

where ω_{ie}^n denotes the projection of the earth rotation rate in the navigation frame. Similarly, ω_{en}^n denotes the angular rate of navigation in the navigation frame. ω_{ij}^j denotes the angular rate in the body frame. ω_{in}^n denotes the angular rate of the navigation frame in the inertial frame articulated in the navigation frame. Q_j^n denotes the quaternion that is attained by attitude. T_a and T_b denote the correlation time, and $\omega 1$ and $\omega 2$ denote the Gaussian white noise processes.

$$\begin{aligned}&\lambda_u\left(\omega_{ij}^j\right) = \begin{bmatrix}0 & -\omega_{ijx}^j & -\omega_{ijy}^j & -\omega_{ijz}^j\\ \omega_{ijx}^j & 0 & \omega_{ijz}^j & -\omega_{ijy}^j\\ \omega_{ijy}^j & -\omega_{ijz}^j & 0 & \omega_{ijx}^j\\ \omega_{ijz}^j & \omega_{ijy}^j & -\omega_{ijx}^j & 0\end{bmatrix},\\ &\lambda_d\left(\omega_{in}^n\right) = \begin{bmatrix}0 & -\omega_{inx}^n & -\omega_{iny}^n & -\omega_{inz}^n\\ \omega_{inx}^n & 0 & -\omega_{inz}^n & \omega_{iny}^n\\ \omega_{iny}^n & \omega_{inz}^n & 0 & -\omega_{inx}^n\\ \omega_{inz}^n & -\omega_{iny}^n & \omega_{inx}^n & 0\end{bmatrix},\\ &G\left(Q_j^n\right) = \begin{bmatrix}-q_1 & -q_2 & -q_3\\ q_0 & -q_3 & q_2\\ q_3 & q_0 & -q_1\\ -q_2 & q_1 & q_0\end{bmatrix},\\ &Y\left(Q_j^n\right) = \begin{bmatrix}-q_1 & -q_2 & -q_3\\ q_0 & q_3 & -q_2\\ -q_3 & q_0 & q_1\\ -q_2 & -q_1 & q_0\end{bmatrix}.\end{aligned} \tag{19}$$

5.4. Cubature Kalman Filter (CKF) Based on the INS/UQ. The state equation and measurement equation of the system are given as

$$\begin{cases}x(t) = f(x(t-1)) + \omega(t-1),\\ z(t) = h(x(t)) + v(t),\end{cases} \tag{20}$$

where $f(x(t-1))$ and $h(x(t))$ are the known functions of the system, $\omega(t-1)$ denotes the system noise, and $v(t)$ is random measure noise. With the help of a sampling point, this filter approaches the distributing function. It also internments features of random variables after the transformation of a nonlinear system. This filter also creates the basic points with the help of the SRC rule. Basic points under the rule are written as

$$\begin{cases}\tau^i = \sqrt{n}\,[1]_i,\\ \omega^i = \dfrac{1}{2_{n_x}},\end{cases}\quad \therefore i = \{1,\ldots,2n\}, \tag{21}$$

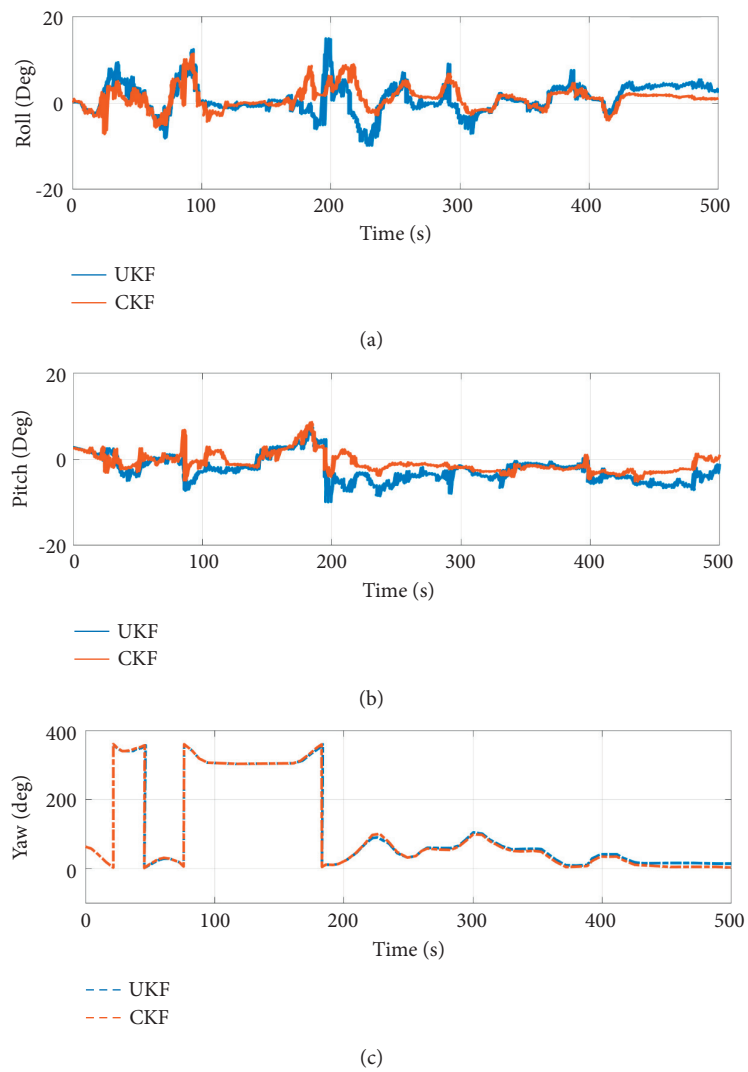

Figure 2: Estimation of EA.

Table 1: Position and orientation errors.

Algorithm	Longitude (m)	Latitude (m)	East (m/s)	North (m/s)	Heading (deg)
UKF	9.7	10.3	4.8	1.5	2.8
CKF	4.3	4.0	2.0	0.8	0.9

where n denote the measurement of state parameters. 1 defines the holohedral point set. The process of the CKF filter is defined as follows.

5.4.1. Time Update. The cubature points that are generated, prediction of state, diffusion of cubature points, and state prediction covariance matrix are given as follows:

$$\begin{aligned} X^i_{(t-1)} &= \sqrt{E(t-1)}\tau^i + \hat{x}(t-1), \\ \overline{x}(t) &= \frac{1}{2n}\overline{X}^i_{(t-1)}, \\ \overline{X}^i_{(t-1)} &= f\left(X^i_{(t-1)}\right), \\ E(t|t-1) &= \frac{1}{2n}\overline{X}^i_{(t-1)}\left(\overline{X}^i_{(t-1)}\right)^T - \overline{x}_t x_t^T + Q(t-1). \end{aligned} \tag{22}$$

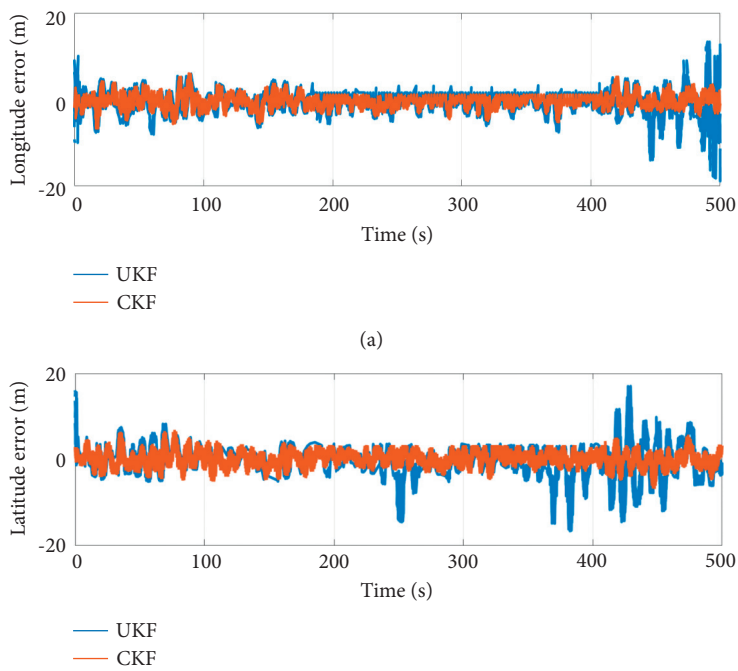

Figure 3: Estimation error of latitude and longitude.

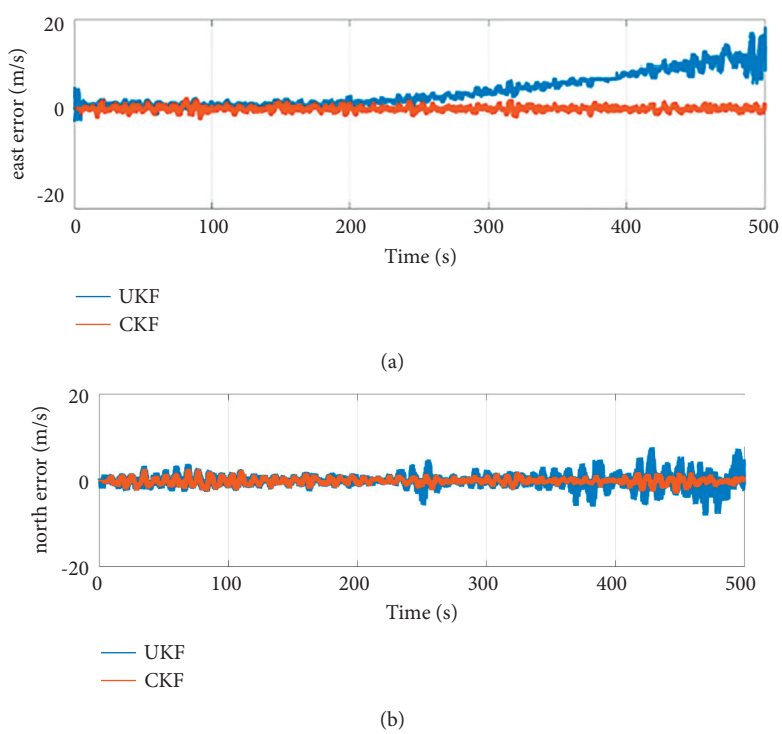

Figure 4: Estimation error in velocity (east and north).

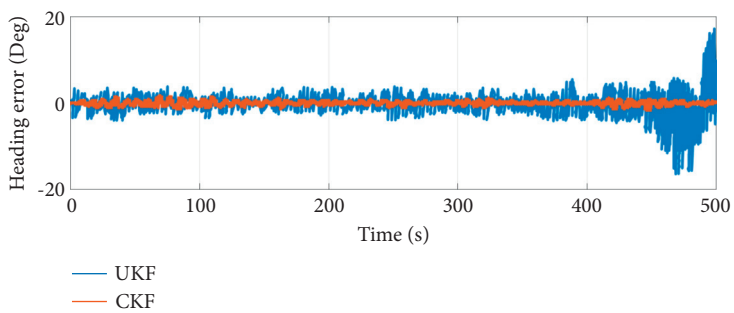

Figure 5: Estimation error of heading.

5.4.2. Measurement Update. The calculation and transmission of cubature points, measurement prediction, innovation covariance matrix, cross-correlation matrix, filter gain matrix, current state estimation, and error covariance matrix calculation are given as follows:

$$\begin{aligned}
\overline{X}_t^i &= \sqrt{E(t|t-1)}\tau^i + \overline{x}(t),\\
\overline{z}^i_{(t|t-1)} &= \frac{1}{2n}\overline{z}^i_{(t|t-1)},\\
E(z(t)) &= \frac{1}{2n}\overline{z}^i_{(t|t-1)}\left(\overline{z}^i_{(t|t-1)}\right)^T - \widehat{z}(t|t-1)\widehat{z}^T_{(t|t-1)},\\
E(x(t)z(t)) &= \frac{1}{2n}\overline{X}^i_t\left(\overline{z}^i_{(t|t-1)}\right)^T - \widehat{z}^T_{(t|t-1)}\overline{x}(t),\\
L(t) &= E(x(t)z(t))E^{-1}_{z(t)},\\
\widehat{x}(t) &= \overline{x}(t) + L(t)(z(t) - \widehat{z}(t|t-1)),\\
E(t) &= E(t|t-1) + L(t)E(z(t))L_t^T.
\end{aligned} \tag{23}$$

6. Simulations and Discussion

This section of the manuscript analyzed the designed scheme based on the set of simulation data received from the movement of the UAV over 500 s. The simulation aims to confirm the applicability of the designed algorithm for short and long runs. This section offers the simulations of the UKF and CKF to prove the effectiveness of each designed technique. The simulations run on the computer with the processor of Intel Core-i7, 16 GB RAM, and 64-bit operating system. MATLAB software was used for the computational simulations.

Two different filters are analyzed and examined in this section. The red line denotes the CKF and the blue line shows the UKF. These two filters solve the common challenges faced during the regular operation. EA estimated from the UKF and CKF is presented. The sensor installed in the UAV provides the readings which help in initializing the integrations. The performance of the system depends upon the environment in which the operation takes place. It is clearly shown in Figure 2 that the CKF has a better performance as compared to the UKF. In roll and pitch, the oscillations are much more as compared to yaw angle. But in comparison to both algorithms, the CKF achieves higher accuracy and stability. In the simulation process, the UKF takes a higher processing load.

Table 1 provides the position and orientation errors averages for fifteen runs. It was done to analyze the reliability of both approaches. The results showed that the CKF provides the best position and orientation as compared to the UKF. Figure 3 shows the longitude and latitude errors recorded. The period of error recorded is 8 min approximately. As shown in figure, the CKF shows less error as compared to others concerning time. Similarly, in Figure 4, the velocity against north and east is defined based on the UKF and CKF. Both velocities are calculated and by the algorithms and with the real parameters. It is shown in figure clearly that east velocity increases after 220 s in the UKF, while in the CKF, the value remains constant near to zero. In north velocity, the error ratio of the UKF is more as compared to the CKF. Last, Figure 5 shows the estimation error of the heading. The figure clearly shows that the error span of the UKF ranges from ±4 to ±15, while the CKF remains nearly to zero. This section defines the reliability and accuracy of the designed approach. Based on the results obtained, the CKF provides the best results as compared to the UKF.

7. Conclusion

This research study presents the design of a nonlinear Kalman filter for the attitude estimation of fixed-wing UAVs. The simulation of the proposed scheme, i.e., AE-UKF and INS-CKF was carried out. The simulation results show that the CKF algorithm can increase the precision of vehicles, and it is inherently nonlinear as compared to other designed algorithms. In many cases, both algorithms show the same results, but the CKF is more precise, having a better nonlinear performance, higher accuracy, and better filter stability. The most important advantage of the CKF is that it is easy to implement.

7.1. Future Enhancement and Limitations. The experimental results show that the proposed scheme in this study increases the accuracy and precision of the fixed-wing UAVs. It solves the attitude estimation problems, and the approach is novel. The future recommendation is that the studies should focus on establishing more accurate and effective techniques for

the attitude estimation of fixed-wing UAVs. The schemes also solve all the problems related to attitude estimation and angle effectively.

This study attains some limitations which are as follows.

(i) First, the proposed scheme only solves the attitude estimation problems

(ii) Second, the projected elements of the state vector are real numbers

(iii) Third, the proposed scheme does not solve the external disturbance issues

(iv) Finally, the study only explores the attitude estimation of fixed-wing UAVs, and this design leaves the possibility of attitude errors in some cases.

Data Availability

The data used to support the findings of this study are included within the article.

Conflicts of Interest

The authors declare that they have no conflicts of interest.

References

[1] I. U. Khan, "Comparitative analyis of IPVE & IPV6 intended for learning object repository to setup an e-learning environment," *Sir Syed University Research Journal of Engineering & Technology*, vol. 11, no. 1, 2021.

[2] B. Alzahrani, O. S. Oubbati, B. Ahmed, M. Atiquzzaman, and D. Alghazzawi, "UAV assistance paradigm: state-of-the-art in applications and challenges," *Journal of Network and Computer Applications*, vol. 166, Article ID 102706, 2020.

[3] M. B. Stuart, A. J. S. McGonigle, and J. R. Willmott, "Hyperspectral imaging in environmental monitoring: a review of recent developments and technological advances in compact field deployable systems," *Sensors*, vol. 19, no. 14, Article ID 3071, 2019.

[4] M. A. Adegboye, W. K. Fung, and A. Karnik, "Recent advances in pipeline monitoring and oil leakage detection technologies: principles and approaches," *Sensors*, vol. 19, no. 11, Article ID 2548, 2019.

[5] L. Chang, F. Qin, and M. Wu, "Gravity disturbance compensation for inertial navigation system," *IEEE Transactions on Instrumentation and Measurement*, vol. 68, no. 10, pp. 3751–3765, 2018.

[6] C. Shen, Y. Zhang, X. Guo et al., "Seamless GPS/inertial navigation system based on self-learning square-root cubature Kalman filter," *IEEE Transactions on Industrial Electronics*, vol. 68, no. 1, pp. 499–508, 2020.

[7] Y. Liu, X. Fan, C. Lv, J. Wu, L. Li, and D. Ding, "An innovative information fusion method with adaptive Kalman filter for integrated INS/GPS navigation of autonomous vehicles," *Mechanical Systems and Signal Processing*, vol. 100, pp. 605–616, 2018.

[8] M. Shafiq, Z. A. Ali, and E. H. Alkhammash, "A cluster-based hierarchical-approach for the path planning of swarm," *Applied Sciences*, vol. 11, no. 15, Article ID 6864, 2021.

[9] A. C. B. Chiella, B. O. S. Teixeira, and G. A. S. Pereira, "Quaternion-based robust attitude estimation using an adaptive unscented Kalman filter," *Sensors*, vol. 19, no. 10, Article ID 2372, 2019.

[10] Y.-jun Yu, X. Zhang, and M. Sadiq Ali Khan, "Attitude heading reference algorithm based on transformed cubature Kalman filter," *Measurement and Control*, vol. 53, no. 7-8, pp. 1446–1453, 2020.

[11] J. Gośliński, W. Giernacki, and A. Królikowski, "A nonlinear filter for efficient attitude estimation of unmanned aerial vehicle (UAV)," *Journal of Intelligent and Robotic Systems*, vol. 95, no. 3, pp. 1079–1095, 2019.

[12] K. R. Gonzales, D. L. Swain, K. M. Nardi et al., "Recent warming of landfalling atmospheric rivers along the west coast of the United States," *Journal of Geophysical Research: Atmospheres*, vol. 124, no. 13, pp. 6810–6826, 2019.

[13] Z. A. Ali, A. Israr, E. H. Alkhammash, and M. Hadjouni, "A leader-follower formation control of multi-UAVs via an adaptive hybrid controller," *Complexity*, vol. 2021, Article ID 9231636, 16 pages, 2021.

[14] A. R. Vetrella, G. Fasano, D. Accardo, and D. Accardo, "Attitude estimation for cooperating UAVs based on tight integration of GNSS and vision measurements," *Aerospace Science and Technology*, vol. 84, pp. 966–979, 2019.

[15] T. Kim, J. Kim, and S.-W. Byun, "A comparison of nonlinear filter algorithms for terrain-referenced underwater navigation," *International Journal of Control, Automation and Systems*, vol. 16, no. 6, pp. 2977–2989, 2018.

[16] W. Youn and B. Matthew, "Rhudy, Am Cho, and Hyun Myung. Fuzzy adaptive attitude estimation for a fixed-wing UAV with a virtual SSA sensor during a GPS outage," *IEEE Sensors Journal*, vol. 20, no. 3, pp. 1456–1472, 2019.

[17] Á Odry, I. Kecskes, P. Sarcevic, Z. Vizvari, A. Toth, and P. Odry, "A novel fuzzy-adaptive extended Kalman filter for real-time attitude estimation of mobile robots," *Sensors*, vol. 20, no. 3, Article ID 803, 2020.

[18] W. You, F. Li, L. Liao, and M. Huang, "Data fusion of UWB and IMU based on unscented kalman filter for indoor localization of quadrotor UAV," *IEEE Access*, vol. 8, pp. 64971–64981, 2020.

[19] X. Yin, X. Peng, G. Zhang, B. Che, and C. Wang, "Flight control system design and autonomous flight control of small-scale unmanned helicopter based on nanosensors," *Journal of Nanoelectronics and Optoelectronics*, vol. 16, no. 4, pp. 675–688, 2021.

[20] F. Al-Turjman, H. Zahmatkesh, I. Al-Oqily, and R. Daboul, "Optimized unmanned aerial vehicles deployment for static and mobile targets' monitoring," *Computer Communications*, vol. 149, pp. 27–35, 2020.

[21] A. Alcántara, J. Capitán, R. Cunha, and A. Ollero, "Optimal trajectory planning for cinematography with multiple unmanned aerial vehicles," *Robotics and Autonomous Systems*, vol. 140, Article ID 103778, 2021.

[22] L. Chen, M. Yuan, L. Zhao, and S. Dong, "Real-time attitude estimation algorithm of flapping-wing air vehicle under large vibration," in *Advances in Guidance, Navigation and Control*, pp. 4609–4621, Springer, Singapore, 2022.

[23] I. Ullah, S. Qian, Z. Deng, and J.-H. Lee, "Extended kalman filter-based localization algorithm by edge computing in wireless sensor networks," *Digital Communications and Networks*, vol. 7, no. 2, pp. 187–195, 2021.

[24] G. Laupré and S. Jan, "On the self-calibration of aerodynamic coefficients in vehicle dynamic model-based navigation," *Drones*, vol. 4, no. 3, Article ID 32, 2020.

Hindawi
International Journal of Optics
Volume 2022, Article ID 4287346, 17 pages
https://doi.org/10.1155/2022/4287346

Research Article

Process Plant Upgradation Using Reliability, Availability, and Maintainability (RAM) Criteria

Dongqiao Bai,[1] **Qi Yang**,[2] **Jian Zhang**,[1] **and Shouzhi Li**[1]

[1]*Xi'an Jiaotong University City College, Xi'an 710018, Shannxi, China*
[2]*Xi'an Microelectronic Technology Institute, Xi'an 710000, Shannxi, China*

Correspondence should be addressed to Dongqiao Bai; bdq1025@163.com

Received 9 November 2021; Accepted 22 December 2021; Published 13 January 2022

Academic Editor: Bhagwan Das

The objective of this study is to propose a solution for process plant upgradation becoming extinct due to obsoleteness of spares. The study will help in reliability, availability, and maintainability (RAM) based upgradation of control system of process plants in developing countries. Available options for plant upgradation are compact control, modular, and semiautomatic. RAM based upgradation provides solution which is high in reliability and availability (usually all parts are replaced with upgraded and compatible technology) and is easy to maintain throughout the service life of process plant. Case study for stacker and reclaimer of cement plant upgradation is considered to both implement and evaluate the idea. Upgradation methodology is finalized by expert's feedback regarding selection of hardware with respect to availability, market survey to validate the opinion, and economical availability viability of selected hardware. Pre- and postupgradation scenarios are analyzed to validate the implementation of study and conclude the expected outcomes. The process plant upgradation yielded a cost-effective solution to the problem with automation increasing by 17%, plant maintainability increasing by 80%, and downtime of plant decreasing by 17%. Among all available options, modular design Op1 is considered the best choice that can satisfy RAM criteria.

1. Introduction

In process plant, different disciplines, such as electrical, instrumentation, automation, and mechanics, depend on each other. Consequently, the development of cross-disciplinary success factors in automated production systems (aPS) requires rigorous investigation [1]. The complication of automation in aPS containing software and hardware is creating a continuously increasing problem in the process industry (cement, fertilizer, chemical, food, and beverages). Modern trends in aPS largely depend upon small sizes, mass customization, higher unpredictability types of products, and a variability product portfolio in factory automation and process plant [2]. Currently the large-scale technology plays a crucial role in diminishing traditional technology, meeting the contemporary timelines, and increasing the size of the industry; however, this could be possible by using categorically competent programmed and well trained staff. Pakistani industry is confronting the difficulty of obsoleteness which is major cause of shutdown of the industry or producing lower quality products and these products lack the potential to compete in international markets [3]. Process accuracies of any industrial unit depend upon the mechanism of mechanical parts and installed control system, its performance, and its accuracy. Both the product and process quality depend on executed process which requires quality control schemes and their implementation by using modern control system such as object oriented programming techniques and modular design [4].

The basic objective of the study is to select the optimal alternative among various options such as compact box, modular design, and semiautomatic option; meanwhile further these options contain subaspects of cost, efficiency, maintenance, and breakdown. First, the compact control system (mostly single module interfacing with all inputs and outputs and centrally processing) has high cost, high efficiency, difficult maintenance, and less breakdowns [5]. Second, the modular option is characterized by low cost, low

efficiency, easy maintenance, and less breakdowns. The third option contains the semiautomatic options having low cost and efficiency, complicated maintenance, and high breakdowns [6]. These are not the only decision criteria; the important thing is where we can apply certain technique. A CNC machine upgradation might be easy to handle with compact control system, while a process plant might have some limitations in implementation due to a variety of IOs and communication issues. In few cases, we might have to compromise on modular approach in few sections because hardware is not compatible for automation and portion if it is operated manually. The improvements in the field of electronic and electrical innovation have been so advanced that various technologies have gone obsolete and supplanted with new innovative ones. The application of advanced surface mount devices (SMD) and application specific integrated circuits (ASICs) have replaced most of the old parts because they have reduced the cost, require less space, and brought new design in field of electronics. The mechanical innovations have made the problems of practicality of the current enterprise frameworks due to obsoleteness of components such as an inaccessibility of hardware, highly priced management frameworks, and repair issues due to unavailability of old mechanical parts that need replacement due to deterioration [5].

New technology is moving towards disposing a particular part after certain lifetime without going for replacement. The problem of accuracy in mechanical processes and methods of first rate of the object exclusively relies upon control framework of any mechanical plant. Relatively small industry is being obscured to the current mechanical devices or maybe current plants which are facing expensive control systems, maintainability problems, and unavailability of hardware [4]. There is a dire need to explore some factors which may be created to spare the end of present mechanical flowers and give them a framework that settles viability problems. Especially the situation is noticeably horrific in developing countries like Pakistan where both the plants are refurbished or semiautomatic or have troubles of destitute preparation control [7]. This leads the plants to face troubles like viability, accessibility of spares/obsoleteness, and high maintenance expenses. In return, plants performance and quality of product decline if we keep on compromising these issues, finally resulting in complete breakdown [8].

Pakistani industry is considered as a traditional industry, with most of plants being second-hand or very old, and few remained shut down due to energy or maintenance crises. However, experts who have been working in similar situation come up with innovative ideas of upgradation or part replacement to make it functional. Concept of bath tub curves of reliability explains that electronics are worst if new due to high infant mortality rate and mechanics are worst if old due to wear and tear plus deterioration of moving parts. Most of the mechanical plant life (manual or semimanual) is outdated because of maintainability issues. Productivity, product quality, and the process accuracy are being compromised and manufacturing sector is paying huge price in the form of quality, cost, benchmark level productivity, and so forth [9]. The major reason for process and quality compromise is that either different automation or process control parts (electronic sensors, modules, processors, or control cards) are obsolete and not available and to keep plant running process automation is bypassed [10]. In order to overcome this problem, we need to come up with some solution that can overcome these obsoleteness issues [11].

The objective of this study is to train and instruct the local process automation industry to develop some upgradation technique using the same process flow but with implementation using different hardware that is more reliable and easily available, thereby increasing plant maintainability [12]. There is a close coordination with similar industry and continuous replacing of obsolete parts with equivalent readily available parts or process modification. The modular technique for the development of process control upgradation design has been carried out and then data concerning reliability of plant, downtime of plant, productivity improvement, and process development has been collected. The objective of this study is to train and instruct the organization performing the task of the automation industry and upgradation of industrial process plants by selecting most suitable and optimal solution among compact control box, modular option, and semiautomatic option based on cost, efficacy, and maintainability issues [10].

For upgradation, we need to study similar process and problem faced by them due to these spares' unavailability and obsoleteness. With selection of replacement, their performance evaluated by similar experts will enhance or knowledge database availability of spares. These are just the prerequisite to make your upgradation task easy which can fulfill RAM criteria. Data regarding plant upgradation is analyzed using some statistical tool; we used Fuzzy Technique for Order of Preference by Similarity to Ideal Solution (F-TOPSIS) to rank the best option for process plant upgradation. F-TOPSIS ranks the best option (among compact control box, modular design, and semiautomatic option) combining the respondents; the study will address the following as well:

(1) To figure out maintainability problem of process plants and key performance indicators (KPIs) being affected

(2) To study and explore the maintainability problem and its effects on process by comparing the pre- and postupgradation scenario established by KPI's improvement and vice versa

(3) To design the strategies for control upgradation which increase the process plant's maintainability and reliability, thus improving performance of the manufacturing in process plant

When we talk about modular approach of upgradation, we want to make sure that a problem in particular area or process of plant might not affect the complete plant or process. Modular approach helps us in separating problematic area and sometimes also helps us to bypass the

problem to decrease the downtime. In old plants, this is necessary to decrease downtime of process plant significantly.

The rest of the paper is organized as follows: Section 2 contains the literature review of the proposed study, Section 3 explains the methodology used in this research, Section 4 elaborates the results and discussions obtained, and Section 5 presents conclusion of the study.

2. Literature Review

Various researchers have been concerned with the characterized practicality such as "the likelihood that a failed framework may be repaired in a selected intervening time of downtime." Lee et al. [13] have defined maintainability as the basic objective of design for maintainability (DFM) is to ensure the maintenance of the product throughout its life-cycle at suitable cost. Existing literature shows [3] that the requirements of maintainability can be categorized as quantitative and qualitative, while both types of maintainability requirements have been used to define the characteristics of maintainability in a system. The overall objective of design maintainability is to reduce costs, ensure safety, and reduce risk, in addition to reliability, availability, maintainability, and supportability (RAMS) [14]. Reliability centered maintenance (RCM) is an essential tool for implementing and scheduling maintenance techniques [15, 16]. RCM is especially effective in frequent failures which causes more time delays; it reduces the life-cycle cost and increases the life-cycle profit. Sillivant [17] suggested that the applications of preventive maintenance are similar in industrial plants. Sondalini [18] conducted the remedial maintenance as next stage from preventive maintenance and it can be defined as follows: once the item is failed, we usually replace it with another one. Based on the existing configuration techniques, Mehairjan [19] proposed that the risk assessment and management system (RAMS) is based on the results of a powerful database, which can indicate the proposed method and work plan to achieve the objectives of RAMS database. It can collect literature to establish an up-to-date database that can determine the fault nature of process system. Stenström et al. [20] identified the weak links, failure rate, and remedial measures in the equipment according to the experience of different users. Mkandawire et al. [21] proposed a method of inputting information in RAMS database in order to correctly format the faults in the list.

Chopra et al. [22] pointed out the quality tests and quality assurance procedures in order to ensure the reliability over a specified period of time under given conditions, whereas reliability becomes more beneficial concerned in testing instrument. Morris et al. [23] stated that, for a system having maintainability problems, its quality and reliability cannot be assured, whereas, for a system having maintainability issues, initial design can be reentered for correction of the problem. Stenström et al. [24] concluded that most of degradation, failure situation, and or variation of outcomes information is grey, whereas the database lacks clarity and consequently RAMS database is facing similar issues. Cheng et al. [9] pointed out that the major problem associated with O&M of process industry is log of maintenance, while minor changes are made by technicians to keep plants running which hook up together to create reliability issues and cause major failure sometimes. Process plant upgradation planning problems encompass uncertain structure due to various options having the contradictory objectives. Fuzzy MCDM approach has the advantage of choosing the best possible alternative, whereas Fuzzy TOPSIS can be transformed into fuzzy numbers having the capability with uncertainty in option choices. However, the application of Fuzzy VIKOR (F-VIKOR) method can be used to choose and categorize the options and recognize the best offer [25,26]. Consequently, the F-VIKOR tool will be used to assess the various choices in order to choose the best possible option. It focuses on prioritizing the options in order to select the solutions of a problematic decision having the contrary criteria. These existing studies have used numerous applications of Fuzzy TOPSIS in various applications. Various researchers have conducted different studies; however, they lack the pre- and postupgradation survey together with the application of Fuzzy Technique for Order of Preference by Similarity to Ideal Solution (F-TOPSIS) to rank the best option for process plant upgradation.

3. Research Methodology

Reliability is the probability of the process functioning without chance of failure during the given time interval under specified conditions [27]. Higher costs lead to engineering solutions to reliability problems for decreasing commercial expenses, increasing reliability, and satisfying customers with quality products, on-time deliveries by reducing cost, increasing equipment availability, and handling the problems arising from products that fail easily [28]. Improving reliability involves decreasing the frequency of process system failure. Improving reliability means decreasing the measure of the probability for failure-free operation, and mathematically it can be shown as

$$R(t) = e^{(-(t/MTBF))} = e^{(-\lambda t)}. \tag{1}$$

Reliability of system with series components is expressed as follows:

$$R\,(\text{reliability of system}) = R1\,(R \text{ of component } 1) \times R2\ (R\,of\ component\ 2) \times \ldots. \tag{2}$$

Reliability of system with parallel components is expressed as follows:

$$\begin{aligned} R\,(\text{reliability of system}) &= 1 - R1\,(R \text{ of component } 1) \\ &\quad \times R2\,(R \text{ of component } 2) \\ &\quad \times \ldots, \\ \text{reliability} + \text{unreliability} &= 1. \end{aligned} \tag{3}$$

3.1. Availability. Availability is the probability of a process system being available when required and it can be represented as a percentage of total time [29]. Mathematically, it can be expressed as

$$\begin{aligned} &\text{Total time} = \text{MTBF}\,(\text{cruel time between failure}) + \text{MTTR}\,(\text{cruel time to settle a disappointment}), \\ &\text{availability} = \frac{\text{time operational}}{\text{total time}} = \frac{\text{MTBF}}{\text{MTBF and MTTR}}, \\ &\text{availability} = \left(1 - \left(\frac{\text{MTTR}}{(\text{MTBF} + \text{MTTR})}\right)\right), \\ &\text{availability} + \text{nonavailability} = 1. \end{aligned} \tag{4}$$

3.2. Maintainability. Maintainability is a significance of design and installation which can be expressed as the probability that an item will be restored or retained for a stated condition within a specific time period [30]. Maintainability analysis has been used to assess the outline and design related to resource requirements and maintenance procedures. Generally the characteristics of maintainability are determined by design of the equipment's set, while the order of maintenance procedures define the time span required for maintenance or repairs. The major characteristic of maintainability is the mean time to repair (MTTR) which shows the ease with which software or hardware can be reinstated to operational state [31]. Quantitative maintainability is the total downtime for maintenance comprising all the time needed for identification of problem, trouble-shooting, active repair time, disassembling, and replacement/removal, verification testing of adequate repair, logistic-movement delays, and administrative tardiness.

$$\begin{aligned} M(t) &= 1 - e^{(-(t/\text{MTTR}))} = 1 - e^{(1-\mu t)}, \\ \text{maintainability} &+ \text{nonmaintainability} = 1, \end{aligned} \tag{5}$$

where μ is a constant characterized by maintenance rate and MTTR is the mean time to repair. MTTR is easy to imagine as compared to probability value. It is anticipated to attain short repair times in order to ensure that the availability remains high. Three main parameters regarding downtime are active repair time, logistic time, and administrative time [32]. Figure 1 shows research methodology path flow for identification of hardware required for plant upgradation and RAM data analysis in parallel with plant upgradation.

Figure 2 shows the practicality square chart of stacker and reclaimer plant with respect to process flow. More detailed is the process flow design; more maintainable is the upgraded solution.

There are numerous unanswered questions considering the whole situation, so we need to know what sort of questions will ensure the correct idea of the situation. Many research methods and investigation strategies are available; nevertheless, there is a need to choose the technique which explores the relationship between the conventional control systems that have reliability and maintainability issues and when the plants are upgraded with most reliable and maintainable control system. The following are the main steps taken to complete this study selection of organization, data sampling questionnaire designing, and the selection of KPIs that need to be asked in survey [33]. Various performance measures for reliability and maintainability have been used in the process industry. Most popular indicators are on-stream factor with slowdown, on-stream factor, turnaround rate, availability (inherent, achievable, or operational), annualized dispatch index, and routine maintenance cost index. Obviously these indicators are used in the operational stage, whereas a few of these indicators can be used to assess different designs. Availability is the ability of an item to accomplish its necessary function at a stated time frame, in order to achieve a high level of availability for plant operations which ensure the profitable status for the manufacturing sector. Generally the process plant availability can be categorized into numerous types such as achievable, operational, and inherent. In essence, the availability of plant operations rejects system availability containing planned and unplanned maintenance time while time is lost to operative logistics and administration.

An achievable availability rejects planned and unplanned availability of maintenance time. The inherent availability

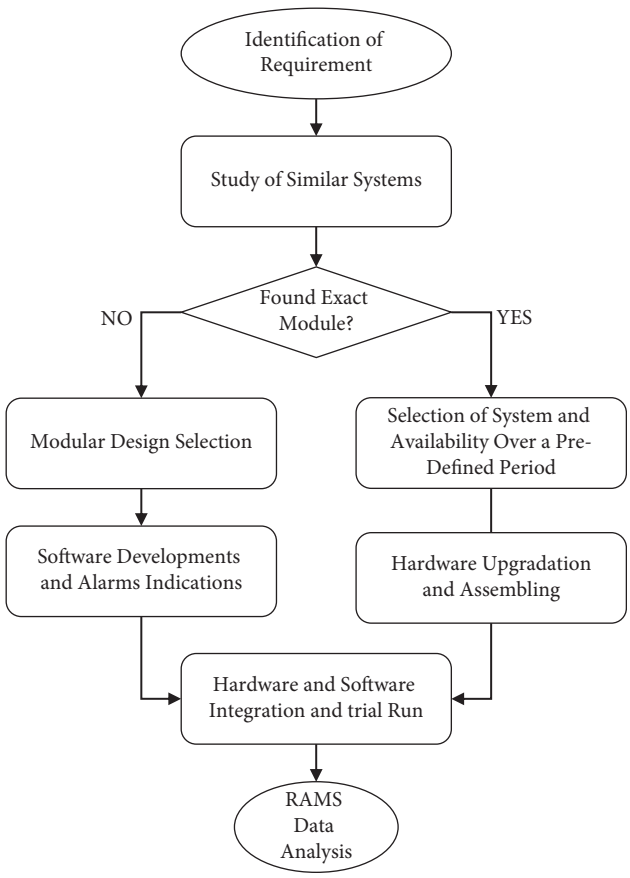

Figure 1: Schematic diagram of research methodology.

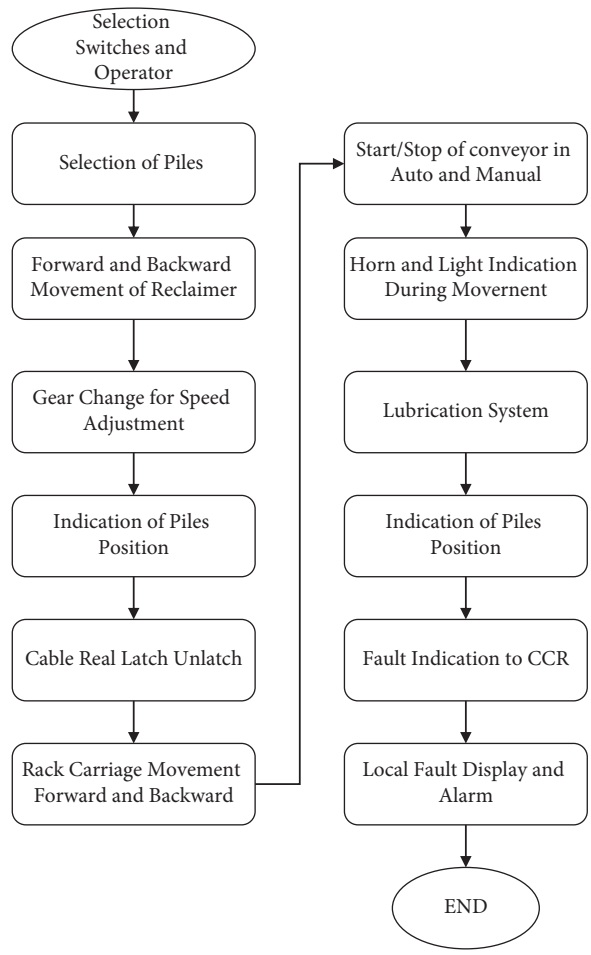

Figure 2: Schematic graph of investigation strategy.

assessment of process plant only evaluates the availability that can be expected when taking into account unprepared maintenance. The most realistic and operational availability is less important in design assessments as administrative and logistics downtime which is outside the control of the designer. Plant availability is considered as the function of the characteristics of reliability and maintainability of process plant. Maintainability actually is the capability of an item to be retained or restored to a condition, in which it can perform its obligatory functions during the maintenance process and using prescribed procedures and resources. Postupgradation responses show that a process engineer can increase the process plant availability at the stage of design development by enhancing maintainability or reliability or both. Although the problem of increasing plant availability stage of design development is relatively complex because several decisions can contribute to plant's maintainability and reliability characterized throughout its life cycle, at this stage, simple short-cut process models have been used for screening purposes, while the assumptions are made about the operational logistics and future control strategy. Within the conceptual stage of the engineering process, additional layers of complexity are added to the process plant models to relax basic engineering assumptions. The process model evolves from the conceptual stage to the engineering stage; a simple risk assessment and management (RAM) systems model can be constructed at the conceptual stage at the defined later stages. The development of a simple RAM model has been used at the conceptual stage which can also be used in combination of the process model to provide preliminary conceptual RAM targets. It can be used to support design engineers making critical design decisions. Figure 3 completely explains the RAM methodology and sequence.

3.3. Reliability and Durability. The basic step in any service is to identify the problem and it can be done by testing where a test stimulus is applied to module or to the system and the output is investigated to see the test specifications. If the outcomes are not specific, then the analysis needs to separate where the fault has been identified. It needs visibility and assessment of investigation for replaceable item. In order to complete the process, it is necessary to assess the input and output of each module as illustrated in Figure 4. This diagnostic capability provided externally or internally built into the system can reduce the cost of maintenance by saving diagnosis time.

The capability of internal diagnostics depends on inputs from electronic signals, built-in system test BIST, and sensors to control the operating parameter about specification. It can be measured through the fault tree analysis in order to suggest the most likely fault and related

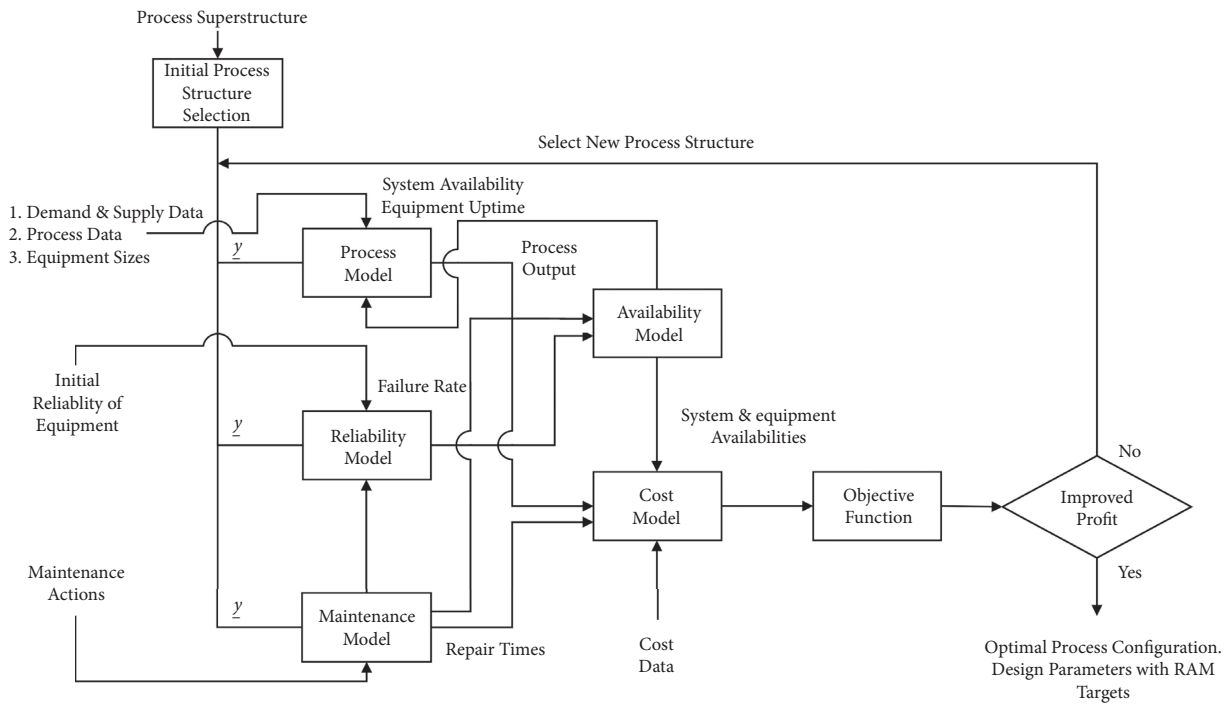

Figure 3: Models interactions: joint integrated process synthesis and availability optimization problem.

maintenance action. Further integration of operating history such as cycles, hours of operations, cycles, and miles can improve the fault tree analysis to the degree that the product is more reliable and durable. The products will require less service. Techniques such as failure reporting, analysis, and corrective action systems (FRACAS) and failure modes and effects analysis (FMEA) can be used to increase the reliability and durability. Reliability of design principles has been found as follows:

(i) Design based on expected range of operating environments

(ii) Provide cabinet AC to all control cabinets where temperature can rise and affect electronics

(iii) Provide critical subsystem redundancy

(iv) Use more reliable/robust parts (industrial grade components are better option)

(v) Reduce part count and interconnections

(vi) Provide modular design making fault isolation and module replacement easy

(vii) The major decisions about enhancing the reliability of a reactor, compressor, and the control system. In our study, we case modular blocks of our control system which is considered active redundancy for the compressor additional control cards for weaker links thereby creating redundancy.

The method of reliability-availability analysis has been used to estimate the availability related parameters for the configuration of given system with maintenance resources, repair characteristics of components, predetermined failure, and the interdependencies between various components. Dismantled parts can be either repaired or supplanted or total module may be changed. Moreover, for a given period of time, there is no issue of obsoleteness and regularly fault reporting components are held in stock to diminish downtime (Figure 5).

3.4. Maintenance Data. Maintenance data provides the equipment date of replacement, date of failure, and maintenance times. Generally the MTTR is calculated from the data which is major contributor to life of process plant. If a plant requires frequent maintenance which shows the low reliability index and low efficiency, this sometime leads us to the decision of replacement and upgradation of plant. The reliability of the device is measured by using Cronbach's alpha coefficient. One essential characteristic of these calculations is that if the data inputs are correlated, then the value of alpha coefficient is increased. Conversely, a high alpha coefficient does not always mean a high degree of validity because alpha coefficient also depends upon the degree of the test. If the length of the test is too short, the value of alpha coefficient is significantly reduced, while the results lose their validity [34]. FMEA have a way to become aware of unsuccessful ways by figuring out weaker links whether they come from layout or from manufacturing. Once we have identified the general failure mode, we can build a solution to avoid it without difficulty. Figure 6 shows the methodology of data collection for RAM criteria and data collection for application of statistic tools.

3.5. Fuzzy Technique for Order of Preference by Similarity to the Ideal Solution (F-TOPSIS). The TOPSIS is a popular method of Multicriteria Decision Analysis (MCDA) in

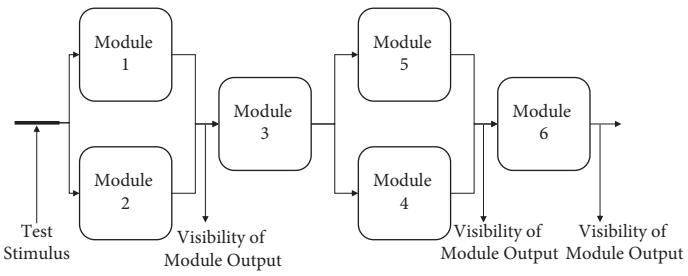

Figure 4: Fault diagnosis internal and external points.

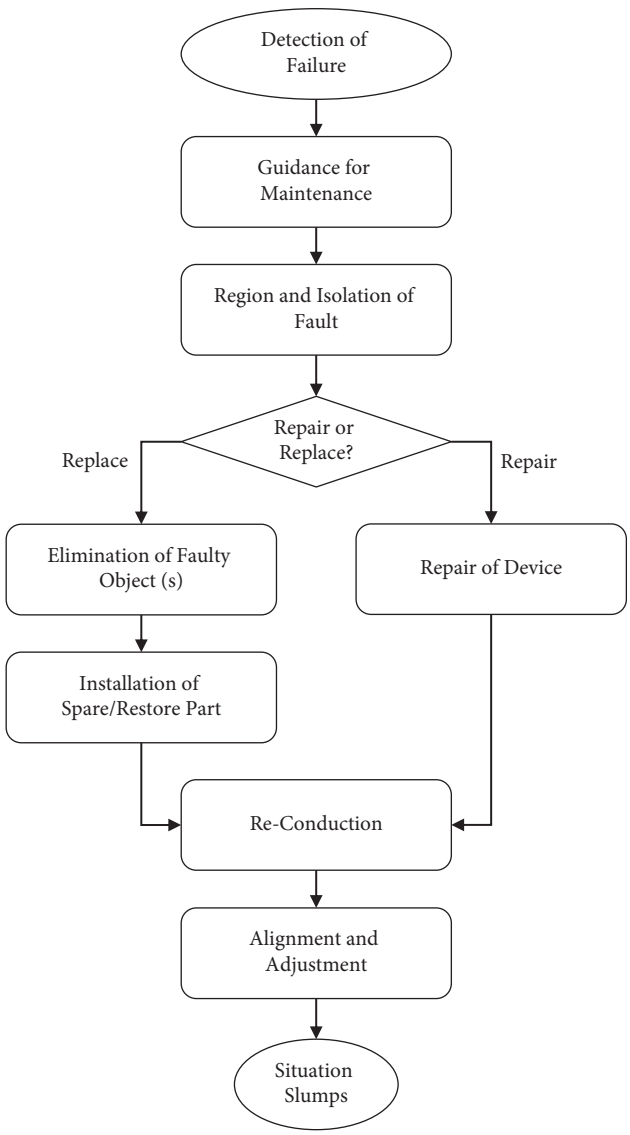

Figure 5: Maintenance cycle of industrial unit.

various applications. The basic objective of this method is to measure the maximum and minimum gaps between positive ideal and negative solutions. However, this method has numerous limitations and indefinite issues and even sometimes fails to ensure the clear information in real-life example. A more significant tool is to assess the various proposed options by means of linguistic variables instead of subjective values. By this, the shift engineers are able to attain an immeasurable and imperfect information through the theory of fuzzy sets. The fuzzy set application was proposed by [35] in economics and engineering. Therefore, the triangular fuzzy number (TFN) is repeatedly being used in MCDA techniques in order to resolve complex problems due to various options. A TFN is a triad $A = (p_u, q_u, r_u)$ where $p_u, q_u, r_u \in \mathbb{R}\,(p_u \le q_u \le r_u)$, having subsequent membership function form:

$$\mu A(x) = \begin{cases} \dfrac{x - p_u}{q_u - p_u}, & \text{if } p_u \le x \le q_u, \\ \dfrac{r_u - x}{r_u - q_u}, & \text{if } q_u \le x \le r_u. \end{cases} \tag{6}$$

The triangular fuzzy numbers (TFNs) have been used to indicate the linguistic variables, which are generally used for the assessment of various options having different criteria. Currently, the TFN rating scale is frequently being used in MCDM problems, shown in Table 1.

The F-TOPSIS technique based on the linguist variables can be obtainable in the following way, where $i = 1, 2, 3, \ldots, m$ and $j = 1, 2, 3, \ldots, n$.

(1) Define the matrix of fuzzy decision X:

$$X = \left(x_{ij}\right)_{m\times n}, \tag{7}$$

where $x_{ij} = (p_{ij}, q_{ij}, r_{ij})$.

(2) Develop the normalized decision matrix of fuzzy numbers M:

$$M = \left[m_{ij}\right]_{m\times n}. \tag{8}$$

Here, $i = 1, 2, 3, \ldots, m$ and $j = 1, 2, 3, \ldots, n$.

$$m_{ij} = \left(\frac{p_{ij}}{r_j^+}, \frac{q_{ij}}{r_j^+}, \frac{r_{ij}}{r_j^+}\right), \tag{9}$$

where $m_j^+ = \max m_{ij}$ (positive i.e., maximum benefit criteria).

$$m_{ij} = \left(\frac{p_j^-}{r_{ij}}, \frac{p_j^-}{q_{ij}}, \frac{p_j^-}{p_{ij}}\right). \tag{10}$$

$p_j^- = \min p_{ij}$ (negative, i.e., smaller the best and cost criteria).

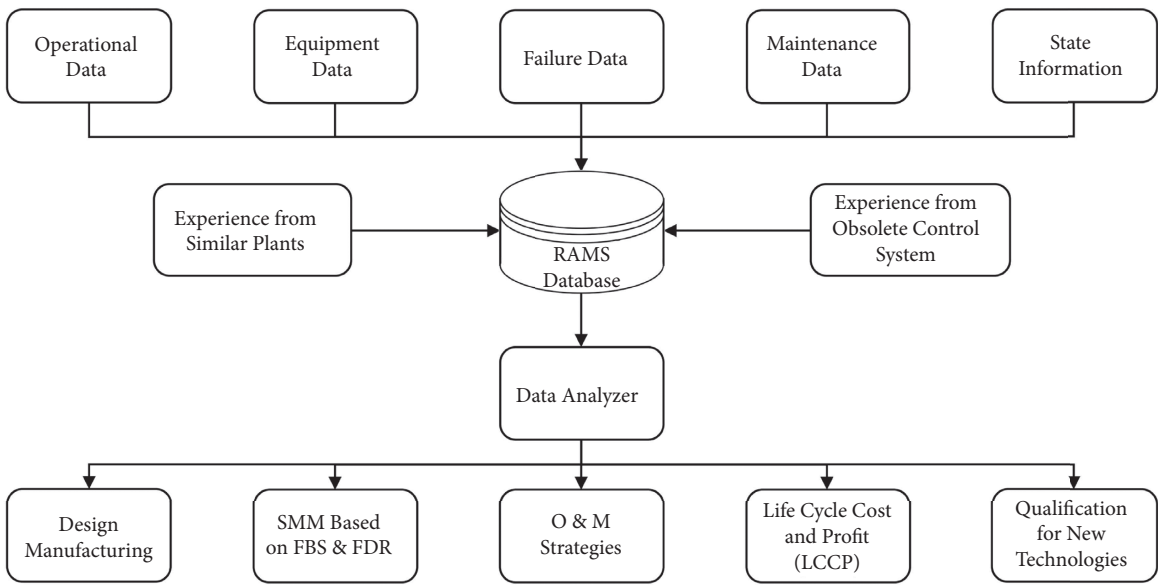

Figure 6: Schematic of proposed RAMS database.

Table 1: Rating scale of linguistic variables and triangular fuzzy number (TFN).

No.	Linguistic variables	(TFN)
1	Very bad (VB)	(1, 1, 3)
2	Bad (B)	(1, 3, 5)
3	Medium (M)	(3, 5, 7)
4	Good (G)	(5, 7, 9)
5	Very good (VG)	(7, 9, 9)

(3) Calculate the weighted normalized fuzzy decision matrix N:

$$N = \left[n_{ij}\right]_{m\times n}. \tag{11}$$

Here, $n_{ij} = m_{ij} \times w_j$.

(4) Identify the fuzzy positive and negative ideal solutions.

$$A^+ = \left(n_1^+, n_2^+, n_3^+, \ldots, n_n^+\right), \tag{12}$$

where $j = 1, 2, 3, \ldots, n$.

$$N_j^+ = \max n_{ij} \text{ if } (j \in J); \quad \min n_{ij} \text{ if } \left(j \in J'\right), \tag{13}$$

$$A^- = \left(n_1^-, n_2^-, n_3^-, \ldots, n_n^-\right), \tag{14}$$

where $j = 1, 2, 3, \ldots, n$

$$N_j^- = \max n_{ij} \text{ if } (j \in J); \quad \min n_{ij} \text{ if } \left(j \in J'\right). \tag{15}$$

(5) Calculate the distances of all alternatives by using equation 18

$$d_i^+ = \sum_{j=1}^{n} d\left(n_{ij} - n_j^+\right), \tag{16}$$

where $j = 1, 2, 3, \ldots$.

$$d_i^- = \sum_{j=1}^{n} d\left(n_{ij} - n_j^-\right), \tag{17}$$

where $j = 1, 2, 3, \ldots, m$.

Now, the distance between the sets of two fuzzy numbers $A = (s_1, s_2, s_3)$ and $B = (t_1, t_2, t_3)$ is

$$d(A, B) = \sqrt{\frac{1}{3}\left[\left(s_1 - t_1\right)^2 + \left(s_2 - t_2\right)^2 + \left(s_3 - t_3\right)^2\right]}. \tag{18}$$

(6) Compute the coefficient closeness (CC_i) of each alternative by using the following equation:

$$\mathrm{CC}_i = \frac{d_i^-}{d_i^+ + d_i^-}, \tag{19}$$

where $i = 1, 2, 3, \ldots, m$; d_i^+ is the distance between the d_i^- fuzzy negative ideal solution and fuzzy positive ideal solution.

(7) Rank and prioritize each optimal option and choose one with higher value of CC_i. The optimal solution and alternative is the one having smaller distances to d_i^+ and d_i^-.

After the completion of the above phases, the F-TOPSIS would guarantee the prioritization and ranking of optimal

alternatives through distance to positive and negative ideal solutions.

3.6. Population and Data Sampling. The population consists of workers from all levels who are specifically included with plant operation and chosen as respondents. To know the results closely related to actual situation, sample survey has been used as a questionnaire to those who have confronted the problems by pre- and postupgradation scenarios. It mainly contains operators, maintenance staff, assistants, shift engineers, repair workers, and front-line managers. The proposed population is helpful to identify significance and its operational capability of the study. In the sampling process, we select the representative of a sample to make the observation neutral and represent the quality of the whole population set [36]. In order to avoid bias sampling in industry, production personnel should ensure that the best samples for quality inspection have very accurate tolerances [37]. Valid, reliable, and unbiased samples need to meet two criteria. Sample must characterize the attributes of the population or target and amount of samples should be adequate to represent the population. In order to evaluate the accurate sample size, the level of precision, the level of confidence, and the degree of variability in the attributes have been measured [38]. Yamane's Formula has been used for sampling purpose and it was selected for determining the sample size. A 95% confidence level and $p = 0.5$ were assumed for equation.

$$n = \frac{N}{\left(1 + N\left(e^2\right)\right)}. \tag{20}$$

Pepsi Cola Lahore has been selected as it has currently upgraded its semiautomatic beverage line to be fully automatic. All parameters concerning reduction in downtime, maintainability, and throughput have been resolved. The personal staff has reduced to 50%.

4. Results and Discussion

A number of overall performance measures have been used in the machine enterprise as signs to explain the overall performance of a plant associated with its reliability and maintainability. The reliability of the instrument has been measured by Cronbach's alpha coefficient which is commonly accepted at the value of 0.60, whereas the sizes of the errors are assessed based on reliability index. For instance, if the reliability of test is 0.6, then error variance comes out to be 0.64 (random error) in the scores ($0.60 \times 0.60 = 0.36$; $1.00 - 0.36 = 0.64$). Usually the system reliability never surpasses component reliability. For a reliability index of 0.8, the error variance value comes out to be 0.36 which is an indication that the reliability of measurement increases and the error variance will decrease [39].

4.1. Preupgradation

4.1.1. Reliability Estimations of Free Variable. Cronbach's alpha coefficient for variables is 0.885. In this study, the variables consist of repairability traceability, local repairing, availability of spares, frequency of faults, concentration/strain stage, alternate solution, user-friendliness, safety, and job security.

In Table 2, there are 10 subfactors of maintainability variables in this study and their Cronbach's alpha coefficient value is given. Respondents' demographic profile for hierarchy stage is shown in Table 3 along with histogram analysis in Figure 7 which shows that about 57.1% of respondents have been working as "operators/assistants" in the groups. About 17.1% of respondents were "preservation personnel (technicians)" within the employer. 14.3% of respondents were "shift engineers" in the organization. Most effective 11.4% of respondents were from "top control" in the corporation.

4.2. Descriptive Analysis. Likert scale data analysis has been performed on interval measurement scale. The mean and standard deviations of all the variables have been measured in order to clarify the respondent responses. The mean and standard deviation of all the variables are given in Table 4. The related histogram analysis is shown in Figure 8. The variable concentration stress level has highest mean value of 4.40 and the standard deviation value is 0.689, whereas the variable alternate solution has the lowest mean value of 1.47 and the standard deviation value is 0.756.

Table 5 shows the amount of traceability. It appears that 45.7% of respondents accept that issues are never traceable. 27.1% of respondents say they are rarely traceable, 15.7% of respondents say they are sometimes traceable, and 5.7% of respondents think they are always traceable.

Table 6 indicates frequency distribution for repairability. It indicates that 38.6% of respondents believe faults are never repairable, 18.6% of respondents believe they are hardly repairable, 24.3% of respondents believe they are sometimes repairable, and 18.6% of respondents believe they are repairable.

Table 7 represents the alternate solution. It appears that 65.7% of respondents said that faults' alternate solution is never available, 34.3% of respondents accepted that alternate solution is rarely available, while 7.1% of respondents accepted that alternate solution is sometimes available, and 2.9% of respondents said alternate solution is often available. Table 8 gives frequency of faults. It shows that 20% of respondents said that faults happen sometimes, 61.4% of respondents stated that faults often occur, and 18.6% of respondents believe that faults always occur. None of the respondents believed that fault rarely occurs which means these plant lifes are often on breakdown and loss of production which is directly proportional to downtime of plant life. This is usually a not unusual phenomenon with aged vintage plants.

Table 9 shows the frequency distribution of safety of preupgradation. It indicates that the majority of respondents considered preupgradation system very dangerous and unsafe. 11.4% of respondents considered it a little bit safe.

Table 10 shows the frequency distribution of job protection security. It indicates that the majority of respondents

Table 2: Reliability statistics.

Cronbach's alpha	No. of items
0.885	10

Table 3: Hierarchy level.

Hierarchy level	Frequency	%
Operators/assistants	40	57.1
Maintenance staff (technicians)	12	17.1
Shift engineers	10	14.3
Top management	8	11.4
Total	70	100.0

considered preupgradation device more jobs secured. In Table 10, 15.7% of the respondents showed neutral response. Since most process and control activities are completed by machines rather than people, job safety is usually compromised by the shift to automation.

Table 11 shows the frequency distribution of repairability. It indicates that the majority of respondents stated faults are always repairable. Due to the modular design method, the modern structure is easy to maintain, so the method of directly replacing the module is often used for maintenance.

Table 12 shows the frequency distribution of concentration level. It indicates that the majority of respondents stated that upgraded systems are stressful. 11.4% of respondents showed a neutral response.

Table 13 shows the frequency distribution of safety from system's hazards. It shows that the majority of respondents stated that upgraded system is usually safe for operation due to automation. A design can be made simpler; the hardware can be reduced considerably. 31.4% of respondents considered safety as often, while 68.6% of respondents said that maintainability always ensures the protection.

In Table 14, independent t-test has been carried out to show the values of frequency along with their sign.

4.2.1. Postupgradation

(1) Descriptive Analysis. Mean and standard deviations of variables are given in Table 14, whereas they are compared in Table 15. The related histogram is given in Figure 9. The variable local repairing has highest value of 5, while the concentration of stress level has a value of 1.57, whereas the standard deviation of the variable local repairing is 0.000 and the standard deviation of job security is 1.57.

Table 16 shows frequency distribution of traceability. It indicates that the majority of respondents said faults are always traceable.

Table 17 shows frequency distribution of repairability. It indicates that the majority of respondents think that the faults are always repairable. Modern systems are easily repairable. Due to the modular design method, this purpose can be achieved by simply replacing parts.

Table 18 shows frequency distribution of local repairing. It indicates that all respondents considered that the faults are always locally repaired.

Table 19 shows the frequency distribution of availability of spares. In indicates that the majority of respondents think that the spares are always available.

In each section of postupgradation, we notice that consequences are leading towards the circumstances that after upgradation plants are repairable and maintainable, and along with this definite other characteristics of user-friendliness and safety can also achieved. The alternate solution in Table 20 shows that the majority of respondents suggested that alternate solution was not needed due to automation.

Table 21 shows frequency distribution of frequency of faults. It indicated that the majority of respondents said that faults rarely occur because of automation.

The user-friendliness table shows that the majority of respondents said that upgraded system is always user-friendly due to automation, whereas very few people who lack education, sufficient knowledge of system, and training considered that it is not user-friendly. However, this was not due to system but due to lack of knowledge of operator (Table 22).

Table 23 shows frequency distribution of concentration/stress level. It indicates that the majority of respondents said that upgraded system requires less concentration and also caused less stress due to automation.

Table 24 shows the frequency distribution of safety. It indicates that the majority of respondents believed that upgraded system is always safe for operation due to automation. A design can be made simpler; the hardware can be significantly decreased by safety and it will be easily maintainable and the cause of maintainability is never accepted or advised. Upgraded system is both more supportable and harmless.

Table 25 shows frequency distribution of job security. It indicates that the majority of respondents said that upgraded system has caused job insecurity.

One-way ANOVA has been used to measure the significant difference in the opinions of respondents because of hierarchy level and time spent in the organization. The results of one-way ANOVA show that there is a significant difference in the opinions of respondents due to hierarchy level and years with organization. In order to measure the difference between means of more than two independent data units, we have used one-way ANOVA to comprehend whether upgradation has influencing factors of alternate solution, repairability, safety, frequency of faults, traceability of faults, local repairing, concentration/stress level, user-friendliness, and job security. The opinions have been analyzed and the results show fluctuated responses based on job level, age group, and experience. One-way ANOVA (Tables 26 and 27) shows that at least last two groups were different. It is similar to collective status concluding that last two were different and not able to differentiate between even any two of them. The one-way analysis of variance (ANOVA) was used to determine whether there is statistical significance.

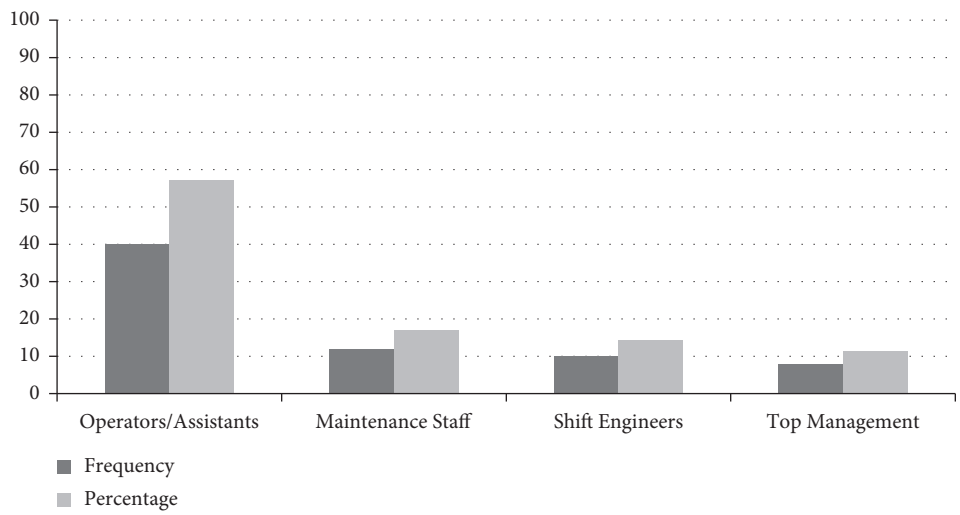

Figure 7: Respondents' demographic profile for hierarchy stage.

Table 4: Descriptive statistics.

Descriptive statistics	*N*	Mean	Std. dev.
Traceability	70	1.99	1.173
Repairability	70	2.23	1.157
Local repairing	70	1.90	0.935
Availability of spares	70	1.54	0.502
Alternate solution	70	1.47	0.756
Frequency of faults	70	3.99	0.625
User-friendliness	70	1.74	0.736
Concentration stress level	70	4.40	0.689
Safety	70	1.63	0.837
Job security	70	3.87	0.658
Valid *N* (list-wise)	70		

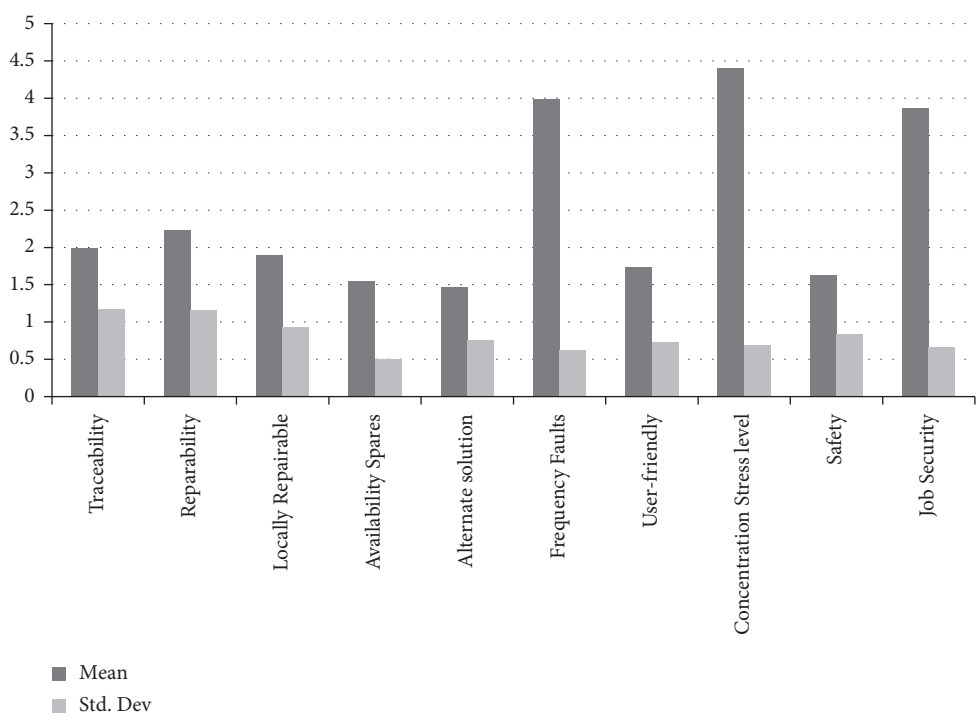

Figure 8: Respondents' demographic mean and standard deviations of all the variables.

Table 5: Traceability.

Traceability	Frequency	%
Never	32	45.7
Rarely	19	27.1
Sometimes	11	15.7
Often	04	5.7
Always	04	5.7
Total	70	100.0

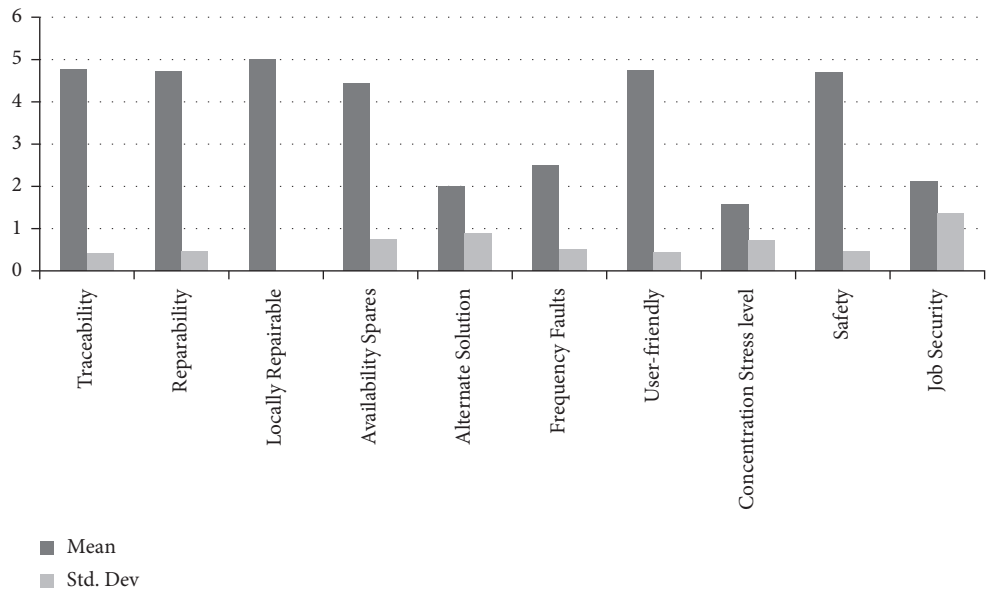

Figure 9: Respondents' demographic profile for hierarchy stage.

Table 6: Repairability.

Repairability	Frequency	%
Never	27	38.6
Rarely	13	18.6
Sometimes	17	24.3
Often	13	18.6
Total	70	100.0

Table 7: Alternate solution.

Alternate solution	Frequency	%
Never	46	65.7
Rarely	17	24.3
Sometimes	5	7.1
Often	2	2.9
Total	70	100.0

Table 8: Frequency of faults.

Frequency of fault	Frequency	%
Sometimes	14	20.0
Often	43	61.4
Always	13	18.6
Total	70	100.0

Table 9: Safety.

Safety	Degree	%
Never	38	54.3
Rarely	24	34.3
Sometimes	4	5.7
Often	4	5.7
Aggregate	70	100.0

Table 10: Job protection.

Job protection	Frequency	%
Rarely	3	4.3
Sometimes	11	15.7
Often	48	68.6
Always	8	11.4
Total	70	100.0

Table 11: Repairability.

Repairability	Frequency	%
Often	20	28.6
Always	50	71.4
Total	70	100.0

Table 12: Concentration/stress level.

Concentration/stress level	Degree/frequency	%
Never	39	55.7
Rarely	22	31.4
Sometimes	9	12.9
Total	70	100.0

Table 13: Safety.

Safety	Frequency	%
Often	22	31.4
Always	48	68.6
Total	70	100.0

Table 14: Independent t-test.

Sr.	Variables	Frequency	Sig.
1	Traceability	8.482	0.005
2	Repairability	153.000	0.000
3	Availability of spares	6.817	0.011
4	Alternate solution	53.691	0.000
5	Frequency of faults	33.333	0.000
6	User-friendliness	6.827	0.011
7	Concentration/stress level	0.482	0.490
8	Safety	0.419	0.520
9	Job security	2.583	0.113

Table 15: Descriptive statistics.

Descriptive statistics	N	Mean	Std. deviation
Traceability	70	4.77	0.423
Repairability	70	4.71	0.455
Local repairing	70	5.00	0.000
Availability of spares	70	4.44	0.735
Alternate solution	70	2.01	0.876
Frequency of faults	70	2.50	0.504
User-friendliness	70	4.74	0.440
Concentration/stress level	70	1.57	0.714
Safety	70	4.69	0.468
Job security	70	2.11	1.357

Table 16: Traceability.

Traceability	Frequency	%
Often	16	22.9
Always	54	77.1
Total	70	100.0

Table 17: Repairability.

Repairability	Frequency	%
Often	20	28.6
Always	50	71.4
Total	70	100.0

Nevertheless, in order to enable reprocessing of several functions, they can be bought up to date and utilized as company specific maintenance. Moreover, on account of standardization of application and basic modules, software

Table 18: Local repairing.

Local repairing	Frequency	%
Always	70	100.0

Table 19: Availability of spares.

Availability of spares	Frequency	%
Sometimes	10	14.3
Often	19	27.1
Always	41	58.6
Total	70	100.0

Table 20: Alternate solution.

Alternate solution	Frequency	%
Never	26	37.1
Rarely	17	24.3
Sometimes	27	38.6
Total	70	100.0

Table 21: Frequency of faults.

Frequency of faults	Frequency	%
Rarely	35	50.0
Sometimes	35	50.0
Total	70	100.0

Table 22: User-friendliness.

User-friendliness	Frequency	%
Often	18	25.7
Always	52	74.3
Total	70	100.0

Table 23: Concentration/stress level.

Concentration/stress level	Frequency	%
Never	39	55.7
Rarely	22	31.4
Sometimes	9	12.9
Total	70	100.0

Table 24: Safety.

Safety	Frequency	%
Often	22	31.4
Always	48	68.6
Total	70	100.0

maintenance is regularly revamped. The company benefits from standardization by introducing automated testing techniques. For reprocessing, some functions can be standardized and used as company specific libraries; the main reason is to keep and make improvement with more effectiveness and efficiency. The standardized application of software can easily improve by company. The main advantage of standardization is to produce large number of software applications. Additionally, different management can be combined into the software development process if

Table 25: Job security.

Job security	Frequency	%
Never	32	45.7
Rarely	19	27.1
Sometimes	5	7.1
Often	7	10.0
Always	7	10.0
Total	70	100.0

Table 26: ANOVA due to hierarchy level.

ANOVA due to hierarchy level		Sum of squares	Df (N-1)	Mean square	*F*	Sig.
Traceability	Between groups	2.743	3	0.914	6.286	0.001
	Within groups	9.600	66	0.145		
	Total	12.343	69			
Repairability	Between groups	3.394	3	1.131	6.856	0.000
	Within groups	10.892	66	0.165		
	Total	14.286	69			
Local repairing	Between groups	0.000	3	0.000	.	.
	Within groups	0.000	66	0.000		
	Total	0.000	69			
Availability of spares	Between groups	16.296	3	5.432	17.093	0.000
	Within groups	20.975	66	0.318		
	Total	37.271	69			
Alternate solution	Between groups	25.611	3	8.537	20.582	0.000
	Within groups	27.375	66	0.415		
	Total	52.986	69			
Frequency of faults	Between groups	13.125	3	4.375	66.00	0.000
	Within groups	4.375	66	0.066		
	Total	17.500	69			
User-friendliness	Between groups	13.371	3	4.457	.	.
	Within groups	0.000	66	0.000		
	Total	13.371	69			
Concentration/stress level	Between groups	11.543	3	3.848	10.76	0.000
	Within groups	23.600	66	0.358		
	Total	35.143	69			
Safety	Between groups	5.186	3	1.729	11.524	0.000
	Within groups	9.900	66	0.150		
	Total	15.086	69			
Job security	Between groups	109.294	3	36.431	135.146	0.000
	Within groups	17.792	66	0.270	000	00
	Total	127.086	69			

the software presently used by the customer is known. As automated testing, kind management and alike programs form a slightly new drift in machine and plant automation, with some aspects, such as quality. Meanwhile software formation and generation can be easier, and the reason is that there are also challenges in this approach because of mechanical restrictions; the machines have a single flow of material. For a new combination of processing stations, the individual modules themselves can be arranged and automatically generated as they work independently from one another.

So far, often process plants and test of machinery can be a lengthy task during the implementation of test requirement. The obstacle is also known as lacking in instrument to maintain for automatic test. In order to test design, the methods of derived testing are often invisible, nonreplicable, and nonstandard and have comprehensive principles, and depend on the intelligence of specific engineers. The subject of quality assurance and testing process can be addressed through the investigation of production process and maintainability. Initially, the procedure of quality process can be addressed, and participants can then be asked whether to apply tests on the device and whether to conduct code reviews. Some companies ensure that there is a trial phase in the software enhancement process to identify faults in a timely manner. In this process, the test processing is carried out, including the equipment and machine flow related to alarm test.

4.3. Fuzzy-TOPSIS Results. The ranking of process plant upgradation has been examined through F-TOPSIS method. The analysis provided by the decision-makers has been developed by the calculation of fuzzy matrix into a TFN by

Table 27: ANOVA due to years with organization.

ANOVA due to years with organization		Sum of squares	Df	Mean square	F	Sig.
Traceability	Between groups	1.293	3	0.431	2.574	0.061
	Within groups	11.050	66	0.167		
	Total	12.343	69			
Repairability	Between groups	2.662	3	0.887	5.038	0.003
	Within groups	11.624	66	0.176		
	Total	14.286	69			
Local repairing	Internal groups	0.000	3	0.000	.	.
	Within groups	0.000	66	0.000		
	Total	0.000	69			
Availability of spares	Between groups	6.738	3	2.246	4.855	0.004
	Within groups	30.533	66	0.463		
	Total	37.271	69			
Alternate solution	Between groups	13.220	3	4.407	7.314	0.000
	Within groups	39.766	66	0.603		
	Total	52.986	69			
Frequency of faults	Between groups	3.373	3	1.124	5.253	0.003
	Within groups	14.127	66	0.214		
	Total	17.500	69			
User-friendliness	Between groups	7.218	3	2.406	25.803	0.000
	Within groups	6.154	66	0.093		
	Total	13.371	69			
Concentration/stress level	Between groups	4.201	3	1.400	2.987	0.037
	Within groups	30.941	66	0.469		
	Total	35.143	69			
Safety	Between groups	2.731	3	0.910	4.864	0.004
	Within groups	12.355	66	0.187		
	Total	15.086	69			
Job security	Between groups	49.502	3	16.501	14.037	0.000
	Within groups	77.584	66	1.176		
	Total	127.086	69			

Table 28: The final ranking of the selected wind sites.

Site	(d_i^+)	(d_i^-)	CC_i	Rank
Op1	16.421	0.612	0.041	1
Op2	14.978	0.587	0.039	2
Op3	14.797	0.578	0.037	3

Table 29: Possible alternatives.

	Complete box	Modular design	Semiautomatic option
Cost	Low	Low	Low
Efficiency	High	Low	Low
Maintenance	Easy	Easy	Complicated
Breakdown	Less	Less	High

the linguistic variables. The linguistic variables of rating matrix were obtained after the comparison of all choices against each of the subcriteria. Subsequently, the matrix of fuzzy normalized decision set, the matrix of fuzzy decision set, and the matrix of fuzzy weighted normalized decision set were obtained through the detailed process of fuzzy decision theory. The ranking of each option, that is, decision alternatives, has been obtained in coordination of coefficient closeness (CC_i) values presented in Table 28.

The present study provides wide-ranging implementation of F-TOPSIS insights and research framework associated with the different methodologies. The outcomes are yielded by enriched methodology with the four major aspects being complete box, modular design, and semiautomatic option and its subaspects to rank the alternatives. All these three underlying options are critical for decision-makers concerning the option selection for upgradation of process plant projects. The results reveal that, in the implementation of Fuzzy-TOPSIS, the selection of process plant upgradation having the bigger CC_i value is prioritized and ranked as the utmost suitable option in order to upgrade the projects. Essentially, results concluded that option 1 (Op1) is considered as the best choice followed by option 2 (Op2) and option 3 (Op3), respectively. This ranking and prioritization of numerous options are critical; in the mean time, experts use scientific decision projects and take into account essential features as well as robust practice. Option 1 (Op1) has satisfactory characteristics across all the relevant features and infrastructure in their surroundings. Essentially, this work can help decision-makers and engineers in the prioritization of feasible option (Table 29).

We have three options, namely, complete box, modular design, and semiautomatic option, further having subaspects of cost, efficiency, maintenance, and breakdown. The

complete box is characterized by low cost, high efficiency, easy maintenance, and less breakdowns. The modular design option is characterized by low cost and efficiency, easy maintenance, and less breakdowns, whereas the semiautomatic option is characterized by low cost and efficiency, complicated maintenance, and high breakdowns.

5. Conclusion and Recommendation

Due to unavailability of the equipment and spares, it is not possible to essentially keep plant running. It has been found that the plants are made functional by using cheaper and most reliable mechanism of control upgradation. The study is implemented on process plant upgradation and the outcome of the study is evaluated. The main focus is not only to evaluate study but also to verify the RAM criteria. Reliability of plant is significantly improved by 80%. Availability and maintainability are increased as the plant is facing less failures, downtime is reduced, and, due to spare availability, plant is more maintainable. Pre- and postupgradation scenarios analysis was conducted involving majority of stakeholders plus experts of the field. The results show that there are specific factors such as frequency of occurrence of faults, traceability, repairability, user-friendliness, maintainability, safety, and job security. Significant improvement has been found after control upgradation in all factors except job security. Modular approach of control design has been facilitated in order to build control system by constructing the independent unit. The fault tracing is made easy by using alarms and spare modules are available and ready to replace without affecting other hardware. Traceability and maintainability are improved and easy as compared to the scenario before upgradation. This has drastically reduced the downtime of plants and improved productivity which has effect on financial position of the firm. This improves the market values of product and production unit. With control upgradation, productivity is enhanced by 17%, plant maintainability is increased by 80%, and downtime of plant is decreased by 17%. Further the results show that option 1 (Op1) is considered as the best choice followed by option 2 (Op2) and option 3 (Op3), respectively. In the future, maintainability may be calculated using the following path for which we want to discover MTBF and MTTR. For this reason, we will have to collect failure records after which reliability tools RCM and λ prediction shall be used. For future work, useful life consumption can be reduced to improve its performance. Overall performance of the proposed database can be enhanced beyond 80%. Significant improvement has been found after control upgradation in all factors except job security. Also fault localization and fault traceability become issues in this study.

Data Availability

The data can be obtained from the corresponding author upon request.

Conflicts of Interest

The authors declare that they have no conflicts of interest.

References

[1] F. Mulubrhan, A. A. Mokhtar, and M. Muhammad, "Integrating reliability analysis in life cycle cost estimation of heat exchanger and pump," *Advanced Materials Research*, vol. 903, pp. 408–413, 2014.

[2] C. Sowmya Danalakshmi and G. Mohankumar, "Analysis of down time and reliability estimation in a process industry—a case study," *International Journal on Design and Manufacturing Technologies*, vol. 3, no. 2, pp. 84–90, 2016.

[3] B. Haughey, "Linking design reviews with FMEA to quickly mitigate the risk of change...design review based on failure modes," in *Proceedings of the Annual Reliability and Maintainability Symposium*, Orlando, FL, USA, January 2017.

[4] P. I. O. Filho, P. Angeli, and E. S. Fraga, "Modelling under uncertainty for process design and scale-up of an industrial AACVD," in *13th International Symposium on Process Systems Engineering (PSE 2018)*, vol. 44, pp. 253–258, Elsevier, Amsterdam, Netherlands, 2018.

[5] J. Zou, J. Arinez, Q. Chang, and Y. Lei, "Opportunity window for energy saving and maintenance in stochastic production systems," *Journal of Manufacturing Science and Engineering*, vol. 138, no. 12, Article ID 121009, 2016.

[6] X.-S. Si, Z.-X. Zhang, and C.-H. Hu, "A real-time variable cost-based maintenance model," *Springer Series in Reliability Engineering*, Springer, Berlin, Germany, pp. 393–404, 2017.

[7] Y. Chiu, C.-H. Yang, and P.-C. Lin, "A just-in-time inventory model with preventive maintenance and defect rate," *International Journal of Information Systems and Supply Chain Management*, vol. 10, no. 4, pp. 44–60, 2017.

[8] J. T. Selvik and E. P. Ford, "Down time terms and information used for assessment of equipment reliability and maintenance performance," in *System Reliability*IntechOpen, London, UK, 2017.

[9] T. Cheng, M. Pandey, and J. van der Weide, "Probability distribution of maintenance cost of a repairable system modeled as an alternating renewal process," in *Advances in Safety, Reliability and Risk Management*, pp. 934–939, Taylor & Francis Group, London, UK, 2012.

[10] C. Letot, P. Dehombreux, E. Rivière-Lorphèvre, G. Fleurquin, and A. Lesage, "A degradation model for maintenance improvement in respect of cost and availability," *Journal of Quality in Maintenance Engineering*, vol. 21, no. 1, pp. 55–69, 2015.

[11] M. Sheikhalishahi, L. Pintelon, and A. Azadeh, "An integrated approach for maintenance planning by considering human factors: application to a petrochemical plant," *Process Safety and Environmental Protection*, vol. 109, pp. 400–409, 2017.

[12] C. Dao, R. Basten, and A. Hartmann, "Maintenance scheduling for railway tracks under limited possession time," *Journal of Transportation Engineering, Part A: Systems*, vol. 144, no. 8, Article ID 04018039, 2018.

[13] A. H. I. Lee, H. Y. Kang, and Y. J. Liou, "A hybrid multiple-criteria decision-making approach for photovoltaic solar plant location selection," *Sustainability*, vol. 9, no. 2, 2017.

[14] D. J. Smith, "The benefits of quantified reliability centred maintenance (ORCM)," *Safety and Reliability*, vol. 15, no. 3, pp. 14–22, 2016.

[15] S. O. Duffuaa, A. Raouf, S. O. Duffuaa, and A. Raouf, "Maintenance material control," in *Planning and Control of Maintenance Systems*, pp. 115–130, Springer, Berlin, Germany, 2015.

[16] S. N. Deakin and I. M. Engineers, "An introduction to reliability-centred maintenance (RCM)," *Des. Reliable Maintenence Railways*, vol. 18, pp. 35–44, 1996.

[17] D. Sillivant, "Reliability centered maintenance cost modeling: lost opportunity cost," in *Proceedings of the Annual Reliability and Maintainability Symposium*, Palm Harbor, FL,USA, January 2015.

[18] M. Sondalini, *Maintenance Cost vs Asset Replacement Value RAV Low Cost Maintenance, World Best Maintenance Practices, World Best Manufacturing Practices, Total Cost of Maintenance*, Lifetime-Reliability Solutions, Rossmoyne, Australia, 2016.

[19] R. P. Y. Mehairjan, "Risk linked reliability-centred maintenance management model," *Risk-Based Maintenance for Electricity Network Organizations*, Springer, Berlin, Germany, pp. 55–81, 2016.

[20] C. Stenström, P. Norrbin, A. Parida, and U. Kumar, "Preventive and corrective maintenance–cost comparison and cost–benefit analysis," *Structure and Infrastructure Engineering*, vol. 12, no. 5, pp. 603–617, 2016.

[21] B. O. B. Mkandawire, N. Ijumba, and A. Saha, "Transformer risk modelling by stochastic augmentation of reliability-centred maintenance," *Electric Power Systems Research*, vol. 119, pp. 471–477, 2015.

[22] A. Chopra, A. Sachdeva, and A. Bhardwaj, "Productivity enhancement using reliability centred maintenance in process industry," *International Journal of Industrial and Systems Engineering*, vol. 23, no. 2, p. 155, 2016.

[23] A. Morris, J. P. Dear, M. Kourmpetis, C. Maharaj, A. Puri, and A. D. Fergusson, "Monitoring creep strain in power station engineering plant," *Applied Mechanics and Materials*, vol. 7, no. 8, pp. 31–36, 2009.

[24] C. Stenström, A. Parida, and U. Kumar, "Structure and infrastructure engineering maintenance, management, life-cycle design and performance preventive and corrective maintenance-cost comparison and cost-benefit analysis preventive and corrective maintenance-cost comparison and cost-benefit analysis," *Structure and Infrastructure Engineering*, vol. 12, 2016.

[25] J. Sofiyabadi, B. Kolahi, and C. Valmohammadi, "Key performance indicators measurement in service business: a fuzzy VIKOR approach," *Total Quality Management and Business Excellence*, vol. 27, no. 9-10, pp. 1028–1042, 2016.

[26] M. Vafaeipour, S. Hashemkhani Zolfani, M. H. Morshed Varzandeh, A. Derakhti, and M. Keshavarz Eshkalag, "Assessment of regions priority for implementation of solar projects in Iran: new application of a hybrid multi-criteria decision making approach," *Energy Conversion and Management*, vol. 86, pp. 653–663, 2014.

[27] M. Mayisela and D. G. Dorrell, "Application of reliability-centred maintenance for dc traction motors - a review," in *Proceedings of the 2019 Southern African Universities Power Engineering Conference/Robotics and Mechatronics/Pattern Recognition Association of South Africa, SAUPEC/RobMech/PRASA 2019*, pp. 450–455, Bloemfontein, South Africa, January 2019.

[28] G. Langli, "Reliability centred maintenance of equipment and systems," in *Operation and Maintenance of Large Infrastructure Projects*, pp. 161–173, CRC Press, Boca Raton, FL, USA, 2019.

[29] L. Dai, M. Rausand, and I. B. Utne, "Availability centred maintenance for offshore wind farms," *Journal of Quality in Maintenance Engineering*, vol. 21, no. 4, pp. 403–418, 2015.

[30] D. J. Smith, "Quantified reliability centred maintenance," in *Reliability, Maintainability and Risk*, pp. 208–214, Elsevier, Amsterdam, Netherlands, 2007.

[31] F. J. Didelet Pereira and F. M. Vicente Sena, "Maintenance functional modelling centred on reliability," in *Condition Monitoring and Diagnostic Engineering Management*, pp. 817–824, Elsevier, Amsterdam, Netherlands, 2007.

[32] B. Dhillon, "Software maintenance and reliability-centered maintenance," in *Engineering Systems Reliability, Safety, and Maintenance*, pp. 179–198, CRC Press, Boca Raton, FL, USA, 2017.

[33] S. Osaki, *Stochastic Models in Reliability and Maintenance*, Springer, Berlin, Germany, 2012.

[34] K. Holmberg and A. Folkeson, *Operational Reliability and Systematic Maintenance*, Routledge, Milton Park, UK, 2018.

[35] G. Q. Chen, S. C. Lee, and E. S. H. Yu, "Application of fuzzy set theory to economics," in *Advances in Fuzzy Sets, Possibility Theory, and Applications*, pp. 277–305, Springer, Berlin, Germany, 1983.

[36] B. Bertsche, "Maintenance and reliability," in *Reliability in Automotive and Mechanical Engineering*, pp. 338–402, Springer, Berlin, Germany, 2008.

[37] J. A. Nachlas, "Predictive maintenance," in *Reliability Engineering*, pp. 287–306, CRC Press, Boca Raton, FL, USA, 2018.

[38] A. K. S. Jardine, *Maintenance, Replacement, and Reliability*, CRC Press, Boca Raton, FL, USA, 2018.

[39] J. R. Sifonte and J. V. Reyes-Picknell, *Reliability Centered Maintenance-Reengineered*, Taylor & Francis, London, UK, 2017.